Available online at www.sciencedirect.com
ScienceDirect
Earth and Planetary Science Letters 265 (2008) 209–228
EPSL
www.elsevier.com/locate/epsl

Stratification and mixing of a post-glacial Neoproterozoic ocean: Evidence from carbon and sulfur isotopes in a cap dolostone from northwest China

Bing Shen [a], Shuhai Xiao [a,*], Alan J. Kaufman [b], Huiming Bao [c], Chuanming Zhou [d], Haifeng Wang [d]

[a] *Department of Geosciences, Virginia Polytechnic Institute and State University, Blacksburg, VA 24061, USA*
[b] *Department of Geology, University of Maryland, College Park, MD 20742, USA*
[c] *Department of Geology and Geophysics, Louisiana State University, Baton Rouge, LA 70803, USA*
[d] *State Key Laboratory of Paleobiology and Stratigraphy, Nanjing Institute of Geology and Paleontology, Chinese Academy of Sciences, Nanjing 210008, China*

Received 4 May 2007; received in revised form 2 October 2007; accepted 3 October 2007
Available online 10 October 2007
Editor: H. Elderfield

Abstract

To improve our knowledge about the geochemical and environmental aftermath of Neoproterozoic global glaciations, we analyzed stable isotopes ($\delta^{13}C$, $\delta^{18}O$, $\delta^{34}S$) and elemental concentrations (Ca, Mg, S, Sr, Fe, and Mn) of the ~10-m-thick Zhamoketi cap dolostone atop the Tereeken diamictite in the Quruqtagh area, eastern Chinese Tianshan. Available chemostratigraphic data suggest that the Tereeken diamictite is probably equivalent to the Marinoan glaciation. Our new data indicate that organic and carbonate carbon isotopes of the Zhamoketi cap dolostone show little stratigraphic variations, averaging −28.2‰ and −4.6‰, respectively. In contrast, sulfur isotopes show significant stratigraphic variations. Carbonate associated sulfate (CAS) abundance decreases rapidly in the basal cap dolostone and $\delta^{34}S_{CAS}$ composition varies between +9‰ and +15‰ in the lower 2.5 m. In the overlying interval, CAS abundance remains low while $\delta^{34}S_{CAS}$ rises ~5‰ and varies more widely between +10‰ and +21‰. The range of $\delta^{34}S_{py}$ of the cap dolostone overlaps with that of $\delta^{34}S_{CAS}$, but direct comparison shows that $\delta^{34}S_{py}$ is typically greater than $\delta^{34}S_{CAS}$ measured from the same samples. Hypotheses to explain the observations must account for both the remarkable sulfur isotope enrichment of pyrites and the inverse fractionation. We propose that CAS and pyrite were derived from two isotopically distinct reservoirs in a chemically stratified basin or a basin with a sulfate minimum zone. In this model, CAS was derived from shallow, oxic surface waters with moderate sulfate concentration and depleted in ^{34}S due to the post-glacial influx of sulfur from continental weathering. In contrast, pyrite was derived from anoxic bottom waters (or a sulfate minimum zone) with low sulfate concentration and ^{34}S enrichment due to long-term syn-glacial sulfate reduction. The rapid shift in CAS abundance and sulfur isotope composition within the cap dolostone is interpreted to reflect the mixing of the two reservoirs after initial deglaciation. Comparison with other post-Marinoan cap carbonates shows significant spatial heterogeneity in $\delta^{34}S_{CAS}$, which together with strong temporal variation in $\delta^{34}S_{CAS}$, points to generally low sulfate concentrations in post-Marinoan oceans.

Keywords: Neoproterozoic; Quruqtagh; cap dolostone; sulfur isotope; carbon isotope; stratification

* Corresponding author. Tel.: +1 540 231 1366; fax: +1 540 231 3386.
E-mail address: xiao@vt.edu (S. Xiao).

0012-821X/$ - see front matter © 2007 Elsevier B.V. All rights reserved.
doi:10.1016/j.epsl.2007.10.005

1. Introduction

Neoproterozoic glacial deposits and immediately overlying carbonates are globally distributed (Evans, 2000; Hoffman and Schrag, 2002), recording severe climatic oscillations. In the snowball Earth model, the world ocean may have been frozen at the equator to a significant depth during glaciation, but rapid warming and extreme oceanic alkalinity during deglaciation resulted in the cap dolostone (Hoffman et al., 1998). The best candidate for such an event is the Marinoan glaciation, which terminated about 635 Ma (Hoffmann et al., 2004; Condon et al., 2005). Most Marinoan glacial deposits are overlain by cap dolostones with characteristic negative $\delta^{13}C_{carb}$ and enigmatic sedimentary features (James et al., 2001; Hoffman and Schrag, 2002; Jiang et al., 2003, 2006; Halverson et al., 2005; Corsetti and Lorentz, 2006; Halverson, 2006; Hoffman et al., 2007; Shields et al., 2007). Collectively, these geochemical and sedimentary features hold the key to understand the aftermath of Marinoan deglaciation.

Current debates on the geochemistry of post-Marinoan oceans have focused primarily on carbon cycle perturbations (Kennedy et al., 2001; Hoffman and Schrag, 2002; Jiang et al., 2003; Halverson et al., 2005; Halverson, 2006), but recent $\delta^{34}S$ studies of sulfides and CAS are providing new insights from the viewpoint of oxidized and reduced reservoirs (Gorjan et al., 2000; Hurtgen et al., 2002, 2004, 2006; Goldberg et al., 2005; Fike et al., 2006; Kaufman et al., 2007; Shields et al., 2007). However, systematic studies of carbon and sulfur isotope fractionation in cap dolostones are generally lacking, and these would likely place important constraints on the biological and physical processes operating in the post-glacial world.

In this study, we carried out high resolution analysis of both carbon and sulfur isotopes in oxidized and reduced phases, along with several major and trace element concentrations, from the ~10 m-thick Zhamoketi cap dolostone. This unit directly overlies the Tereeken diamictite in the Quruqtagh area, eastern Chinese Tianshan, which has been interpreted to be Marinoan in age. Together with previously published data (Xiao et al., 2004), the high resolution geochemical data reported here provide evidence for chemical stratification and subsequent overturn in the Quruqtagh basin and perhaps the world ocean in the aftermath of a widespread Neoproterozoic glaciation.

2. Geological background

The Quruqtagh area belongs to the southeast branch of Chinese Tianshan, and is geologically part of the northern Tarim Block (Gao et al., 1980; Zhang et al., 2007). Neoproterozoic successions in the Quruqtagh area (Fig. 1) were first described as the Quruqtagh Series (Norin, 1937), and later as the Quruqtagh Group (Gao and Zhu, 1984; Gao et al., 1993).

The Quruqtagh Group overlies early Neoproterozoic stromatolitic carbonates, and disconformably underlies basal Cambrian phosphorites/cherts (Yao et al., 2005). It is divided into the Bayisi, Zhaobishan, Altungol, Tereeken, Zhamoketi, Yukkengol, Shuiquan, and Hankalchough formations (Fig. 2a). The >250-m-thick Bayisi Formation consists of phyllite-slate grade metasediments and metavolcaniclastics. Four units of greenish gray diamictite, each ranging from a few to >100 m in thickness and separated by quartz and polylithic metawackes, occur in the Bayisi Formation. Outsized clasts, mostly derived from older metamorphic and igneous rocks, occur in the diamictite. A volcanic unit in the basal Bayisi Formation gives a SHRIMP zircon U–Pb age of 755±15 (1σ) Ma (Xu et al., 2005) and another near the topmost Bayisi Formation has been dated as 727±8 (1σ) Ma (S. Xiao and Z.-X. Li, unpublished data). The Bayisi Formation is succeeded by the 100–300-m-thick Zhaobishan Formation, which consists of metawackes, metarenites, calcareous siltstones, and slates. The overlying Altungol Formation consists of metamorphosed diamictites, metavolcanics, and marbles characterized by $\delta^{13}C_{carb}$ values between +2‰ and +10‰ (Xiao et al., 2004). The ~200-m-thick Tereeken Formation consists of at least five diamictite intervals separated by finely laminated siltstones and mudstones, with abundant dropstones and striated clasts (Fig. 3a) in the diamictites (Gao and Zhu, 1984; Xiao et al., 2004). The siltstone/mudstone intervals may represent interludes of less extensive glacial cover (Leather et al., 2002) and bioproductivity resumption.

The Tereeken Formation is sharply succeeded by a ~10-m-thick cap dolostone in the basal Zhamoketi Formation (Fig. 3b), which is characterized by $\delta^{13}C_{carb}$ values between −4‰ and −6‰ (Xiao et al., 2004). The rest of the Zhamoketi Formation and the overlying Yukkengol Formation consist of ~1200 m of meter-scale cycles of sandstone and siltstone, which are interpreted as deep-water turbidites. The Zhamoketi and Yukkengol formations are demarcated by basaltic and andesitic volcanic rocks. Further upsection is the Shuiquan Formation that consists of <100 m carbonate characterized by a large $\delta^{13}C_{carb}$ shift from −9‰ to nearly 0‰. This shift may be equivalent to the upper part of the Shuram anomaly (Fike et al., 2006).The uppermost Quruqtagh Group is represented by the ~400-m-thick Hankalchough Formation, which consists of light gray

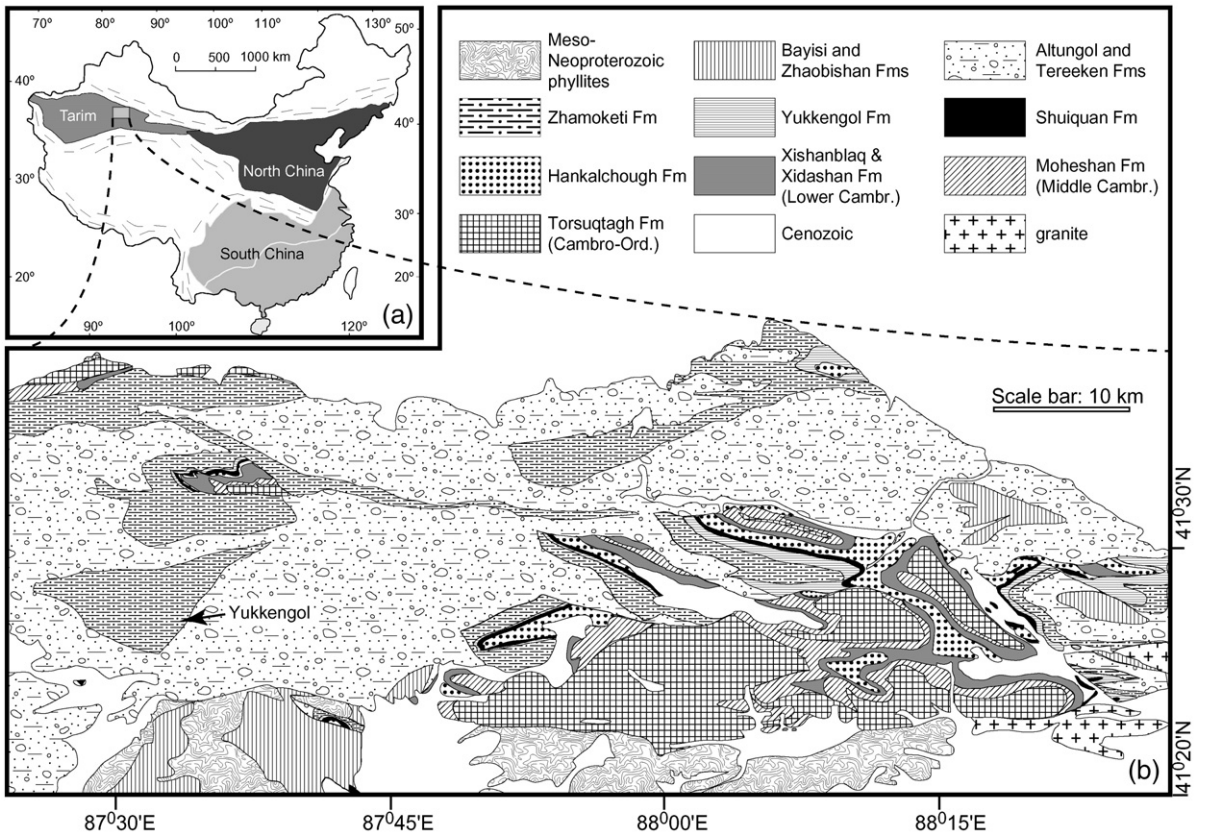

Fig. 1. (a) Geographic location of the Tarim Block. Rectangle indicates area shown in b. (b) Geological map of the Quruqtagh area. Arrow points to location of the Yukkengol section.

diamictite with abundant dropstones and striated clasts (Zhao et al., 1980). A 1–5-m-thick dolostone unit succeeding the Hankalchough diamictite and characterized by variably negative $\delta^{13}C_{carb}$ values is regarded as the Hankalchough cap carbonate. The Hankalchough Formation is overlain disconformably by phosphorites/cherts of the Xishanblaq Formation where basal Cambrian *Micrhystridium*-like acritarchs and small shelly fossils have been reported (Yao et al., 2005).

A glacial origin for diamictites in the Bayisi, Altungol, Tereeken, and Hankalchough formations has been proposed (Gao and Zhu, 1984), although the most convincing glacial evidence comes from the Tereeken and Hankalchoug diamictites, where abundant striated clasts (Fig. 3a) and dropstones are present (Gao and Zhu, 1984; Xiao et al., 2004). Although radiometric ages provide only loose constraints on the Tereeken glaciation (<727±8 Ma), the stratigraphic association of the 727±8 Ma age and the Bayisi diamictite suggests that the Bayisi and Tereeken formations probably record the Sturtian and Marinoan glaciations, respectively. This is consistent with $\delta^{13}C$ chemostratigraphic evidence (Xiao et al., 2004), including (1) the $\delta^{13}C$ stratigraphic pattern of the Zhamoketi cap dolostone, which is more akin to post-Marinoan than to post-Sturtian cap carbonates; and (2) highly positive $\delta^{13}C$ values (up to 10‰) in the Altungol Formation, which may be equivalent to the positive $\delta^{13}C$ excursion between the Sturtian and Marinoan glaciations (Halverson et al., 2005). This correlation implies that the Tereeken glaciation may have terminated about 635 Ma (Hoffmann et al., 2004; Condon et al., 2005).

The focus of this study is the Zhamoketi cap dolostone. Sixty-three samples, at an average spacing of 10–20 cm, were collected at the Yukkengol section (Fig. 1). Here, the Zhamoketi cap dolostone consists of 10-meter-thick pink-colored dolostone or limy dolostone (Fig. 3b). The Zhamoketi cap dolostone can be divided into three lithostratigraphic units (Fig. 2). The lower unit A consists of ~1.2-m-thick thin-bedded calcitic dolomicrosparite. The middle unit B is composed of a 1.5-m-thick macropeloidal dolostone (Fig. 3c) that is lithologically

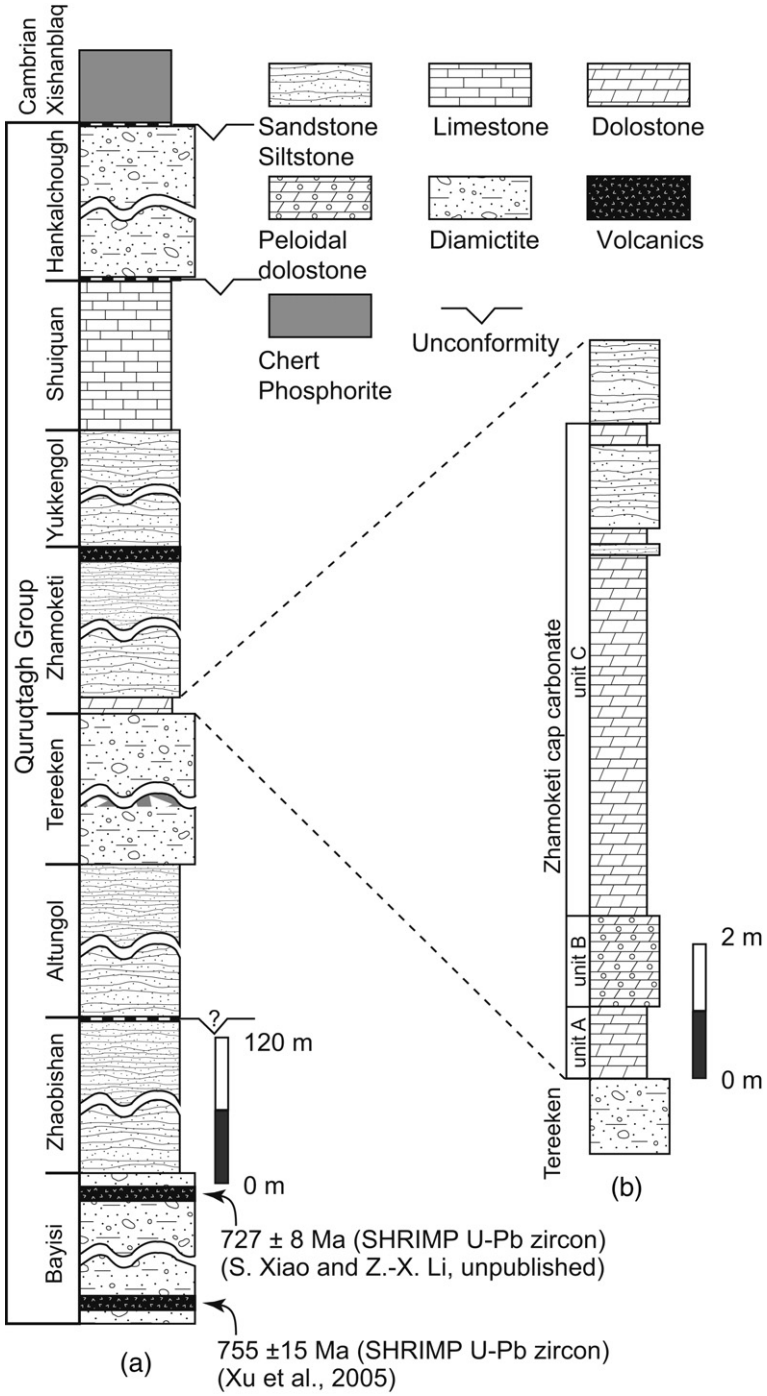

Fig. 2. (a) Stratigraphic column of Neoproterozoic Quruqtagh Group. (b) Detailed stratigraphic column of the Zhamoketi cap carbonate at the Yukkengol section.

similar to macropeloidal dolostones in the Ravensthroat cap carbonate in the Mackenzie Mountains (James et al., 2001), Bwipe cap carbonate in the Volta Basin (Nédélec et al., 2007), and Doushantuo cap carbonate in South China (personal observation). The macropeloids, 0.5–4 mm in diameter, are aggregates of very small peloids. They are cemented by blocky calcite (Fig. 3c; calcite cement representing <10% rock volume). The upper unit C consists of 7-m-thick homogeneous dolomicrosparite (Fig. 3d) and siliciclastic components increase upsection.

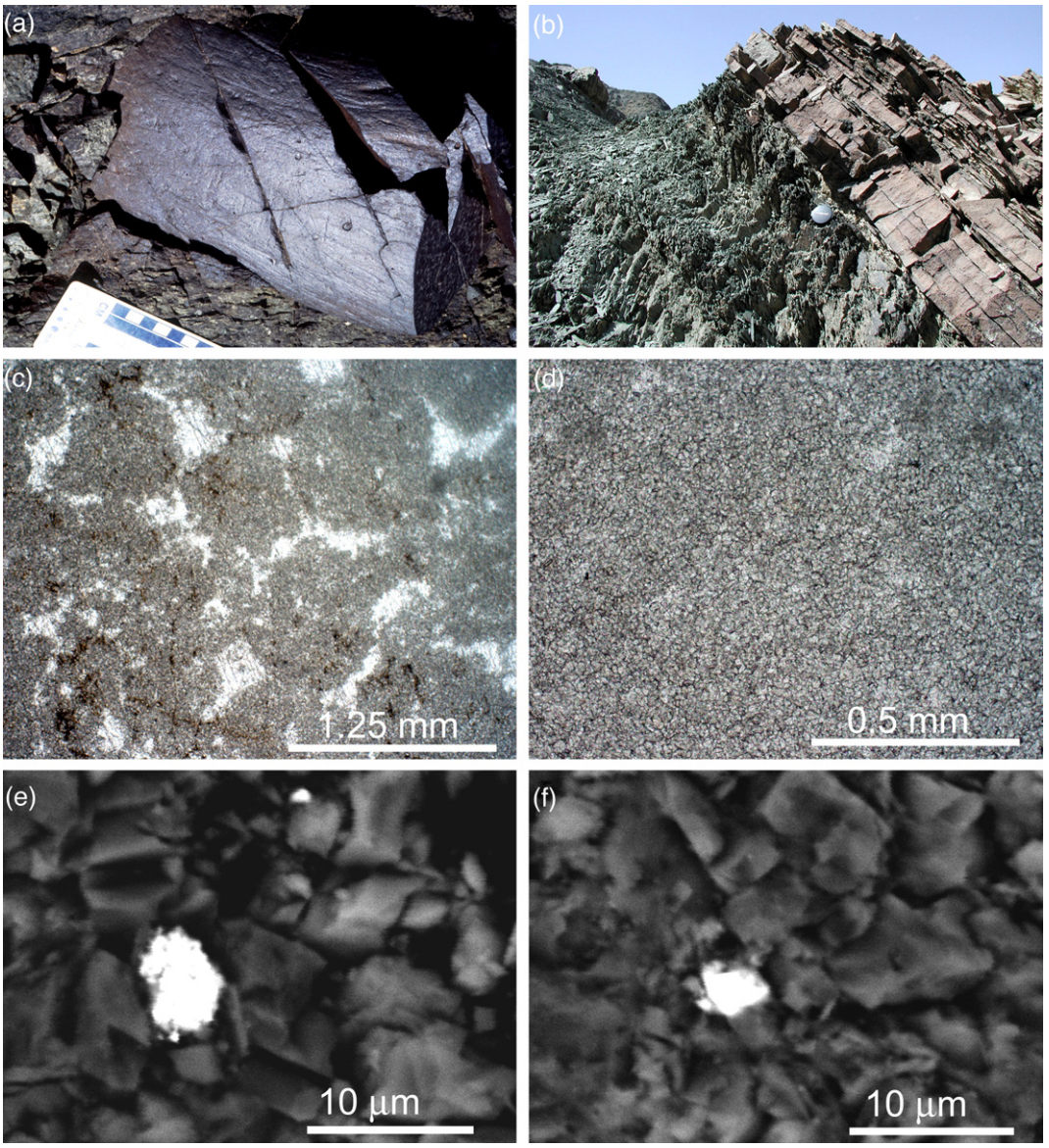

Fig. 3. (a) Striated clast in the Tereeken diamictite. (b) Field photograph showing the sharp contact between Tereeken diamictite and pinkish Zhamoketi cap dolostone at the Yukkengol section. (c) Photomicrograph of macropeloids in the Zhamoketi cap dolostone (unit B; delta-27, 136x11). (d) Photomicrograph of dolomicrite/dolomicrosparite in the Zhamoketi cap dolostone (delta-51, 141.8x11.7). (e–f) Back scattered electron micrographs of disseminated pyrites (bright color) in the Zhamoketi cap dolostone (delta-11).

The Zhamoketi cap carbonate contains a small amount of pyrites, which are disseminated randomly in dolomicrosparite matrix (Fig. 3e–f).

The Zhamoketi cap dolostone was probably deposited below storm wave base. Tepee-like structures, interpreted as giant wave ripples (Allen and Hoffman, 2005), are not present in the Zhamoketi cap dolostone. Nor are other sedimentary structures such as cross stratification, sheet cracks, and tube-forming stromatolites (Corsetti and Grotzinger, 2005) that would indicate sedimentation in the euphotic zone. The lack of enigmatic sedimentary features characteristic of many other post-Marinoan cap dolostones is probably due to the deep-water settings of the Zhamoketi cap dolostone.

3. Methods

3.1. Carbon and oxygen isotopes

$\delta^{13}C_{carb}$ and $\delta^{18}O$ data of the Zhamoketi cap dolostone at Yukkengol were previously published by Xiao et al. (2004), although their stratigraphic resolution

Table 1
Geochemical data of the Zhamoketi cap carbonate at the Yukkengol section

Sample number	Height	$\delta^{13}C_{carb}$	$\delta^{13}C_{org}$	$\Delta\delta^{13}C$	$\delta^{18}O$	$\delta^{34}S_{CAS}$	$\delta^{34}S_{py}$	$\Delta\delta^{34}S$	Fe	Mn	Sr	CAS	Mg/Ca
	(m)	(‰)	(‰)	(‰)	(‰)	(‰)	(‰)	(‰)	(ppm)	(ppm)	(ppm)	(ppm)	(molar)
Δ-10	0.00	−7.8	−24.7	16.9	−15.4	10.3	ns.	na.	4055	5064	930	791	0.04
Δ-11	0.03	−8.3	−27.4	19.1	−16.4	14.5	ns.	na.	2981	4836	657	315	0.44
Δ-12	0.09	−4.9	−28.0	23.1	−10.5	11.1	16.4	−5.4	3709	5481	593	332	0.50
Δ-13	0.12	−4.6	na.	na.	−8.8	11.4	16.0	−4.6	5046	6540	502	253	0.55
Δ-14	0.16	−5.1	−29.0	23.9	−10.1	11.0	ns.	na.	3913	5815	532	829	0.38
Δ-15	0.18	−4.3	−27.8	23.5	−9.0	12.1	15.9	−3.9	2845	4237	456	533	0.53
Δ-16	0.23	−5.4	−25.6	20.2	−11.2	10.3	14.1	−3.8	4513	5828	561	1116	0.42
Δ-17	0.30	−5.9	na.	na.	−10.9	14.0	15.4	−1.3	3302	4590	505	237	0.41
Δ-18	0.33	−5.2	−29.7	24.5	−11.5	12.5	15.5	−2.9	5270	4899	482	535	0.45
Δ-19	0.37	−5.3	−29.1	23.8	−10.6	11.0	14.2	−3.2	4629	4560	449	690	0.47
Δ-20	0.39	−5.1	−26.3	21.2	−11.2	14.0	15.2	−1.3	4888	5570	521	264	0.46
Δ-21	0.48	na.	na.	na.	na.	11.8	ns.	na.	4626	4040	375	430	0.50
Δ-22	0.62	−4.8	−27.9	23.1	−10.8	12.0	11.8	0.2	4262	3999	360	154	0.61
Δ-23	1.00	−4.3	−28.0	23.7	−8.5	11.6	15.3	−3.7	6145	5476	312	173	0.67
Δ-24	1.22	−4.9	−27.6	22.7	−9.8	10.3	13.9	−3.5	4134	4488	281	97	0.66
Δ-25	1.27	−4.8	−28.4	23.5	−8.7	10.6	16.5	−5.9	4350	4836	279	249	0.68
Δ-26	1.38	na.	na.	na.	na.	10.8	ns.	na.	4340	4619	267	414	0.72
Δ-27	1.50	na.	na.	na.	na.	9.1	18.5	−9.4	4435	5101	304	285	0.76
Δ-28	1.63	−4.5	−25.5	21.0	−9.2	12.2	18.3	−6.1	na.	na.	na.	225	na.
Δ-29	1.70	−4.6	na.	na.	−8.7	10.8	16.0	−5.2	3939	5276	320	211	0.71
Δ-30	1.77	−4.6	−26.7	22.1	−9.7	10.8	15.5	−4.7	3603	4629	286	214	0.77
Δ-31	1.82	−4.9	−29.2	24.3	−9.6	12.1	17.4	−5.3	3506	4586	326	188	0.76
Δ-32	1.88	−4.2	−28.7	24.5	−8.5	12.9	15.7	−2.8	4223	4874	291	308	0.78
Δ-33	1.90	na.	−28.9	na.	na.	10.6	16.5	−5.9	4520	5551	333	777	0.75
Δ-34	2.08	−4.5	−27.9	23.4	−8.3	13.1	15.7	−2.6	3983	6079	352	352	0.75
Δ-35	2.12	−4.4	−28.7	24.3	−9.2	12.1	15.9	−3.8	3826	5561	335	262	0.78
Δ-36	2.20	−4.6	−27.6	23.0	−9.3	14.6	15.8	−1.2	4396	5798	365	296	0.79
Δ-37	2.29	−4.4	−27.9	23.5	−8.9	13.4	ns.	na.	4238	5484	333	208	0.78
Δ-38	2.43	−4.3	na.	na.	−8.4	14.0	15.5	−1.5	3781	5446	333	328	0.78
Δ-39	2.54	−4.2	−28.3	24.1	−8.9	20.6	ns.	na.	3760	5386	366	145	0.76
Δ-40	2.68	−4.4	−27.5	23.1	−8.7	12.9	17.4	−4.5	3409	5233	355	378	0.76
Δ-41	2.79	−4.3	−28.8	24.5	−8.9	16.6	17.0	−0.3	3813	5181	357	191	0.78
Δ-42	2.89	−4.3	−29.1	24.7	−8.5	14.4	ns.	na.	4329	5335	415	288	0.76
Δ-43	3.16	−4.4	−28.4	24.0	−9.1	19.6	ns.	na.	4350	5057	395	130	0.77
Δ-44	3.44	−4.2	−28.1	23.9	−8.5	19.3	ns.	na.	3591	4356	359	136	0.75
Δ-45	3.64	−4.5	−28.1	23.6	−9.2	12.8	15.8	−3.0	3656	4230	379	295	0.78
Δ-46	3.80	−4.2	−29.3	25.1	−8.8	12.2	14.6	−2.5	3688	4198	449	374	0.78
Δ-47	3.98	−4.1	−29.3	25.2	−8.8	11.5	16.6	−5.0	3419	4050	381	458	0.80
Δ-48	4.08	−4.1	−27.6	23.5	−8.8	12.7	15.1	−2.4	4116	4293	443	329	0.80
Δ-49	4.25	−4.2	−26.2	22.0	−9.1	16.7	ns.	na.	4112	4253	406	181	0.81
Δ-50	4.34	−4.1	−29.0	24.9	−8.3	19.7	13.1	6.6	4077	4225	396	138	0.82
Δ-51	4.51	−4.3	−28.2	23.9	−9.3	13.3	16.0	−2.7	3193	3747	389	260	0.78
Δ-52	4.60	−4.2	−28.6	24.5	−8.4	19.1	14.6	4.5	3460	3697	359	127	0.83
Δ-53	4.82	−4.1	−29.0	24.9	−10.5	10.6	18.3	−7.7	5555	3951	247	308	0.97
Δ-54	5.45	−4.1	na.	na.	−8.4	16.8	19.5	−2.6	3619	4766	307	164	0.81
Δ-55	5.68	−4.1	−28.4	24.3	−8.8	15.0	ns.	na.	3379	4194	267	189	0.84
Δ-56	5.78	−4.3	−28.9	24.6	−8.9	12.7	ns.	na.	4043	5086	344	329	0.83
Δ-57	5.97	−4.3	−27.7	23.4	−9.1	11.0	ns.	na.	3803	4718	302	475	0.81
Δ-58	6.08	−4.4	na.	na.	−9.1	13.0	16.2	−3.3	3742	4490	344	282	0.80
Δ-59	6.27	−4.1	−28.9	24.7	−8.4	15.4	ns.	na.	3933	4681	376	172	0.82
Δ-60	6.49	−4.3	−28.4	24.1	−9.4	11.7	ns.	na.	4159	4753	366	352	0.84
Δ-61	6.58	−4.2	na.	na.	−9.0	15.2	13.7	1.5	4261	5176	379	152	0.85
Δ-62	6.79	−4.4	−28.7	24.3	−9.7	10.1	16.1	−6.0	4329	4698	451	254	0.81
Δ-63	6.99	−4.0	−29.1	25.1	−8.4	10.1	14.6	−4.5	4586	4678	266	312	0.91
Δ-64	7.15	−4.2	−28.4	24.2	−9.3	13.1	ns.	na.	4956	4609	264	240	0.93
Δ-65	7.21	−3.9	−28.7	24.7	−8.3	15.9	16.0	−0.1	5988	4947	234	158	0.98

Table 1 (*continued*)

Sample number	Height (m)	$\delta^{13}C_{carb}$ (‰)	$\delta^{13}C_{org}$ (‰)	$\Delta\delta^{13}C$ (‰)	$\delta^{18}O$ (‰)	$\delta^{34}S_{CAS}$ (‰)	$\delta^{34}S_{py}$ (‰)	$\Delta\delta^{34}S$ (‰)	Fe (ppm)	Mn (ppm)	Sr (ppm)	CAS (ppm)	Mg/Ca (molar)
Δ-66	7.34	−4.1	−28.7	24.5	−8.3	13.7	ns.	na.	6805	4919	340	213	0.93
Δ-67	7.39	−4.1	−28.4	24.4	−8.2	15.6	15.9	−0.3	6397	4522	267	158	0.95
Δ-68	7.61	−4.1	−28.8	24.7	−9.0	14.1	ns.	na.	6173	4478	207	192	1.00
Δ-69	7.73	−4.2	−28.7	24.5	−8.4	18.8	ns.	na.	6896	4883	216	124	1.00
Δ-70	7.95	−4.1	−28.7	24.6	−7.7	18.9	ns.	na.	7042	5137	227	148	1.00
Δ-71	8.22	−4.4	−28.4	24.0	−9.0	9.7	ns.	na.	4432	4342	547	509	0.01
Δ-72	9.75	−5.2	−29.2	24.0	−9.5	17.1	ns.	na.	8337	5240	233	176	0.95

Footnote: ns: no sufficient yield; na: not analyzed; CAS: carbonate associated sulfate; $\Delta\delta^{13}C=\delta^{13}C_{carb}-\delta^{13}C_{org}$; $\Delta\delta^{34}S=\delta^{34}S_{CAS}-\delta^{34}S_{py}$.

was on the order of 50 cm. To increase the stratigraphic resolution, we analyzed additional $\delta^{13}C_{carb}$ and $\delta^{18}O$ data from Yukkengol section 1 described in Fig. 7a of Xiao et al. (2004). $\delta^{13}C_{carb}$ and $\delta^{18}O$ were measured on drilled microsamples, following procedures described in Xiao et al. (2004). Isotopic results are expressed in the standard δ notation as per mil (‰) deviations from VPDB. Uncertainties determined by multiple measurements of a laboratory standard carbonate (calibrated to NBS-19) were better than 0.05‰ (1σ) for both $\delta^{13}C_{carb}$ and $\delta^{18}O$.

For $\delta^{13}C_{org}$ analysis, 1–2 g of rock chips were first leached with 15% HCl and 10% HF for 15 min, and washed with deionized water three times to remove surface weathering. Washed chips were dried and crushed to 80 mesh. Sample powders were then acidified three times with 6 M HCl to dissolve carbonate. Insoluble residue was centrifuged and washed with deionized water more than three times, and was then dried in an oven at 60 °C. $\delta^{13}C_{org}$ values were determined on decalcified residues by combustion at 850 °C for 2 h with CuO as an oxidant in evacuated and sealed Vycor tubing. CO_2 derived from the combustion was quantified and packaged for mass spectrometric analysis. Results are reported as per mil (‰) deviations from VPDB. Uncertainties based on multiple analyses of a standard carbonate are better than 0.3‰ (1σ).

3.2. Sulfur isotopes

Sulfur isotopes compositions were determined on coexisting sulfide and trace sulfate isolated from the same samples where $\delta^{13}C_{carb}$ and $\delta^{18}O$ were measured. Extraction of carbonate associated sulfate (CAS) followed the procedure of Goldberg et al. (2005). 50–100 g of rock chips were leached with 3 M HCl to remove surface weathering, washed and dried prior to being crushed to 80 mesh. Powders were weighed, leached in 10% NaCl solution for 24 h, and then washed three times with deionized water to remove soluble sulfate. Leached powders were transferred into a 500 ml flask with 50 ml of deionized water, and then dissolved in the flask following a stepwise acidification procedure in which HCl acid was added successively 3 or 4 times. In the first treatment, 20 ml of 10 M HCl was added, and the flask was gently shaken to allow reaction for 20 to 30 min. This step was repeated 2 or 3 times until carbonate was quantitatively dissolved, and final solution was allowed to sit for ~2 h. Insoluble residues were removed by filtration with 1 μm filter paper, carefully washed, dried, and weighed. The volume of supernatant was measured, and then distributed in four 50 ml centrifuge tubes, one of which was used for elemental analysis. Barite was precipitated by adding 1–2 ml of saturated $BaCl_2$ solution to the three remaining tubes and allowing reaction for 48 h. All processed samples precipitated sufficient barite for $\delta^{34}S_{CAS}$ analysis.

Disseminated pyrite was extracted following the chromium reduction method (Canfield et al., 1986; Goldberg et al., 2005). 5–7 g of fresh rock samples was crushed to 80 mesh and powders were reacted with 50 ml of 1 M $CrCl_2$ and 20 ml of 10 M HCl in an N_2 atmosphere. H_2S produced from pyrite reduction by $CrCl_2$ was bubbled through a 1 M zinc acetate trap where it was precipitated as ZnS, which was then converted to Ag_2S by ion exchange with $AgNO_3$. The Ag_2S was centrifuged, washed three times using deionized water, and dried at 60 °C. Twenty-three out of 63 processed samples did not yield a sufficient quantity of Ag_2S for analysis.

Sulfur isotopes were measured in the geochemistry laboratory at University of Maryland. Prepared samples (~100 μg $BaSO_4$ or Ag_2S) were accurately weighed and folded into small tin cups. A Eurovector elemental analyzer (EA) was used for on-line combustion at 1030 °C and separation of SO_2 on-line to a GV Isoprime mass spectrometer for $^{34}S/^{32}S$ analyses, following the procedures of Grassineau et al. (2001). Isotopic results are expressed in the δ notation as per mil (‰) deviations from VCDT. Uncertainties determined by multiple

analyses of a standard barite (NBS 127) are better than 0.3‰ (1σ).

3.3. Elemental geochemistry

Major and trace elemental contents of Ca, Mg, Fe, Mn, Sr, and S were analyzed on an Inductively Coupled Plasma Atomic Emission Spectrometer (ICP–AES) in the Virginia Tech Soil Testing Laboratory. Solutions from the CAS extraction procedure that did not react with $BaCl_2$ were used for elemental analysis. Elemental concentrations were corrected for insoluble residue (by subtracting insoluble residue from sample powder mass), and CAS concentrations were calculated from sulfur abundances. Analytical precision is better than 5% for sulfur and 3% for other elements when they are above the detection limit.

4. Results

4.1. Carbon and oxygen isotopes

The high resolution $\delta^{13}C_{carb}$ and $\delta^{18}O$ data (Table 1; Fig. 4a–b) confirm the stratigraphic pattern reported by Xiao et al. (2004). With the exception of the two lowermost samples, which might have experienced some degree of diagenetic alteration (as indicated by their $\delta^{18}O$ values <-15‰ and close contact to underlying diamictite), $\delta^{13}C_{carb}$ values show little variation. Above the basal samples values start around −4‰ and then fall to near −6‰ at 0.3 m before returning within the macropeloidal unit (unit B) to a plateau value of ca. −4‰. Oxygen isotopes are similarly stable with most values ranging between −8 and −11‰, but do co-vary with carbon isotopes (Fig. 5a).

$\delta^{13}C_{org}$ values (Fig. 4a) range from −29.7 to −24.7‰ ($n=53$, mean=−28.2‰, SD=1‰), again showing very little variation. Fractionations between carbonate and organic carbon are remarkably stable throughout the cap dolostone. Excluding the two lowermost samples, $\Delta\delta^{13}C$ values ($=\delta^{13}C_{carb}-\delta^{13}C_{org}$) range from 25.2‰ to 20.2‰ ($n=50$, mean=23.8‰, SD=1‰), consistent with carbon isotope fractionation by oxygenic photoautotrophs.

4.2. Sulfur isotopes

In contrast to carbon isotopes, $\delta^{34}S_{CAS}$ values show wide variations between +9.1‰ and +20.6‰ (Table 1; Fig. 4c; $n=63$, mean=13.4‰, SD=2.9‰). Closer inspection of the stratigraphic profile reveals a 3–5‰ positive shift and increase in variability at ~2.5 m; this is apparent from statistical analysis (below 2.5 m: $n=29$, range=9.1–14.6‰, mean=+11.9‰, SD=1.4‰; above 2.5 m: $n=34$, range=9.7–20.6‰, mean=+14.7‰, SD=3.1‰). The variability can also be evaluated by examining the absolute difference between successive samples (Fig. 4d; below 2.5 m: mean=1.7‰; above 2.5 m: mean=3.6‰). In contrast, there are no stratigraphic patterns in the mean, range, or variability of $\delta^{34}S_{py}$ values, which vary widely between +11.8‰ and +19.5‰ throughout the cap dolostone (Table 1; Fig. 4e; $n=40$, mean=15.8‰, SD=1.5‰).

The isotopic difference between CAS and pyrite ($\Delta\delta^{34}S_{CAS-py}={}^{34}S_{CAS}-\delta^{34}S_{py}$) ranges from −9.4‰ to +6.6‰ (Fig. 4f; $n=40$, mean=−3.0‰, SD=3.0‰), demonstrating that bulk pyrite is remarkably enriched in ^{34}S relative to trace sulfate of the same samples. In 36 out of the 40 samples, bulk pyrite $\delta^{34}S_{py}$ values are greater than $\delta^{34}S_{CAS}$ values.

4.3. Elemental geochemistry

No persistent stratigraphic trends are apparent in Mn concentrations (3700–6500 ppm), but Fe concentrations (2800–8800 ppm) appear to increase in the upper 3 m of the cap dolostone (Fig. 4h). In addition, Sr (210–930 ppm) and CAS concentrations (100–1100 ppm) decrease in the lowest meter (Fig. 4g–h), whereas Mg/Ca ratios increase (Fig. 4i) in the lowest 2 m, suggesting a transition from calcitic dolomite to stoichiometric dolomite with decreasing Sr and CAS concentrations.

5. Validity of CAS concentration, $\delta^{34}S_{CAS}$, and $\delta^{34}S_{py}$ data

5.1. Pyrite oxidation during laboratory preparation or outcrop weathering

It is conceivable that the extraction of CAS may be contaminated by pyrite oxidation during laboratory preparation or outcrop weathering. However, pyrite concentration in the Zhamoketi cap dolostone is very low. We estimate on the basis of Ag_2S yield that Zhamoketi samples typically contain <20 ppm pyrite (or <10 ppm pyrite sulfur, compared with 30–430 ppm CAS sulfur). In fact, more than a third of processed samples did not yield measurable amount of Ag_2S (<0.1 mg). Controlled experiment by one of us (AJK) has shown that laboratory oxidation of pyrite does occur, but its effect on CAS and $\delta^{34}S_{CAS}$ measurements is negligible when pyrite concentration is low compared to CAS abundance. Outcrop weathering of pyrite would produce sulfate on rock surface or in fractures. But the

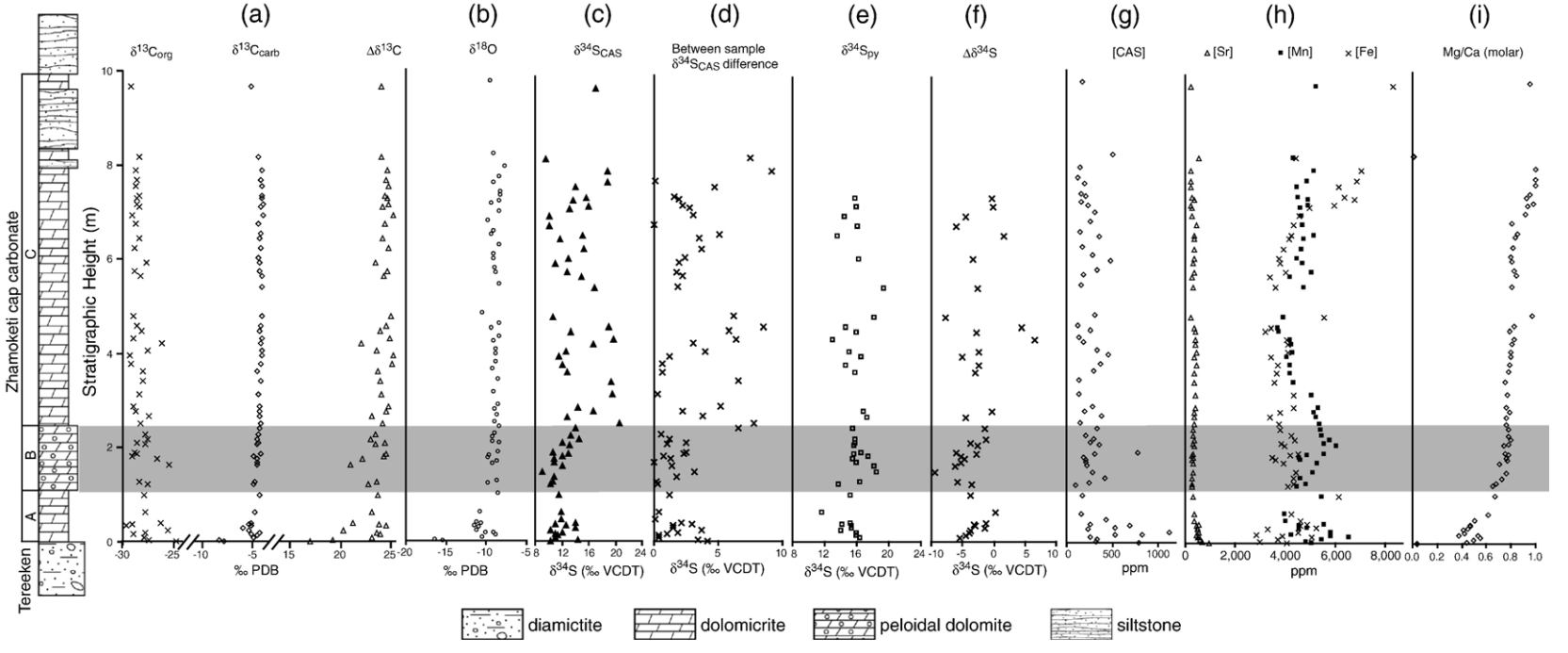

Fig. 4. Isotopic and elemental geochemistry profiles of the Zhamoketi cap dolostone at the Yukkengol section. Between sample $\delta^{34}S_{CAS}$ difference is calculated as the absolute difference in $\delta^{34}S_{CAS}$ between successive samples. $\Delta\delta^{13}C = \delta^{13}C_{carb} - \delta^{13}C_{org}$; $\Delta\delta^{34}S = \delta^{34}S_{CAS} - \delta^{34}S_{py}$.

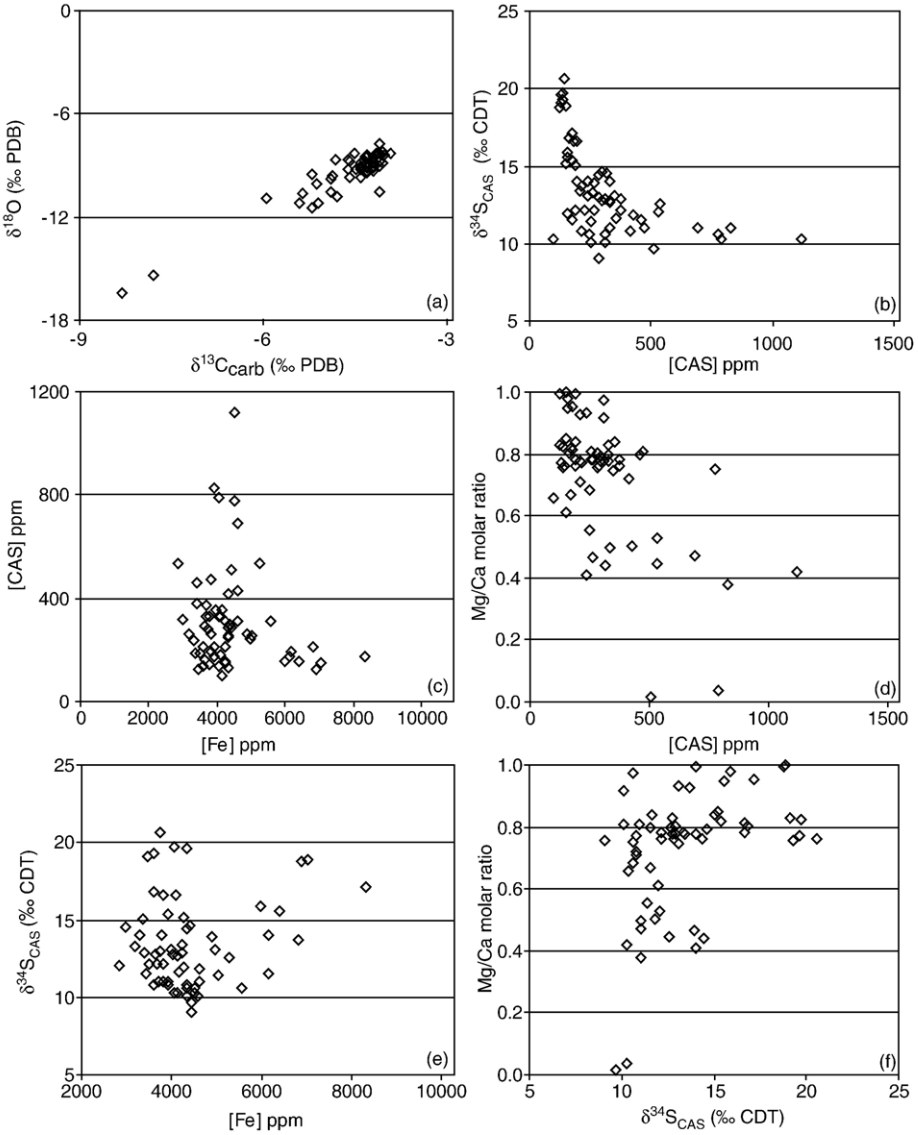

Fig. 5. Isotope and elemental cross-plots.

sample powders were pretreated with 10% NaCl solution, which should remove soluble sulfate derived from outcrop weathering of pyrite.

With regard to the Quruqtagh data reported in this paper, the following consideration argues against significant contamination from pyrite oxidation. Such contamination would lead to a positive correlation between CAS concentrations and $\delta^{34}S_{CAS}$ values insofar as pyrite in these samples has greater ^{34}S abundance than CAS, but our data show a weak negative correlation between CAS concentration and $\delta^{34}S_{CAS}$ (Fig. 5b). Neither is there a positive correlation between Fe and CAS concentrations (Fig. 5c) or between Fe concentration and $\delta^{34}S_{CAS}$ (Fig. 5e), as might be expected if both sulfate and Fe oxyhydroxide from *in-situ* pyrite oxidation were retained in the rock and later liberated in CAS extraction. The lack of these expected geochemical correlations also indicate that the low pyrite concentrations in the Zhamoketi cap dolostone cannot be due to significant oxidative loss of originally abundant pyrite.

5.2. Diagenetic alteration of CAS concentration and $\delta^{34}S_{CAS}$

It is also a concern that $\delta^{34}S_{CAS}$ may have been altered during late diagenesis. CAS can be lost from or

added to carbonates during post-burial diagenesis. Lyons et al. (2004, 2005) have shown that, despite CAS concentrations decreasing from 3500 to 500 ppm in aragonite–calcite inversion during meteoric diagenesis, $\delta^{34}S_{CAS}$ values remained within 1 to 2‰ of the coeval seawater value. Thus, it is reasonable to assume that $\delta^{34}S_{CAS}$ is largely buffered against diagenetic alteration at least during aragonite stabilization.

The effect of dolomitization on CAS concentration and $\delta^{34}S_{CAS}$ has not been completely understood (Lyons et al., 2005). Hurtgen et al. (2006) reported that CAS concentrations of Neoproterozoic dolostones seem to be greater than limestones (contrary to our own observation, Fig. 5d). Hurtgen et al.'s data can be interpreted in two ways. Primary dolomites can have high CAS concentrations if they are precipitated in evaporitic environments and can retain high CAS concentrations due to their greater stability to reduce diagenetic CAS loss. Alternatively, secondary dolomites might incorporate additional sulfate from pore-water during dolomitization. The former interpretation implies that primary dolomites are better proxies for sea water $\delta^{34}S$. The latter interpretation predicts that $\delta^{34}S_{CAS}$ of dolostones be slightly greater than coeval seawater sulfate, because bacterial sulfate reduction in sediments could drive $\delta^{34}S_{\text{pore water sulfate}}$ to be greater than $\delta^{34}S_{\text{seawater sulfate}}$, particularly when sulfate reduction rate is high and diffusion of sulfate into sediment is not facilitated by bioturbation. Indeed, this prediction is consistent with the observation that $\delta^{34}S_{CAS}$ values of dolostones are consistently 3–5‰ greater than interbedded gypsum beds in the Mesoproterozoic Bylot Supergroup (Kah et al., 2004), although this difference between dolostone and gypsum is relatively small compared to stratigraphic variation of $\delta^{34}S_{CAS}$ values.

In the Zhamoketi cap dolostone, there is evidence suggesting that, although CAS concentrations might have altered, the broad secular trends of CAS concentrations are still useful in qualitatively constraining sulfate concentrations in Neoproterozoic oceans. The weak negative correlation between Mg/Ca ratio and CAS concentration (Fig. 5d) indicates possible CAS loss during dolomitization, inconsistent with previous observations that Neoproterozoic dolomites have greater CAS concentrations than limestones (Hurtgen et al., 2006). Regardless, Zhamoketi CAS concentrations (100–1100 ppm; $n=63$, mean=308 ppm, SD=194 ppm; Fig. 4g) are comparable to or slightly greater than other Neoproterozoic or Mesoproterozoic carbonates (Hurtgen et al., 2004, 2005; Kah et al., 2004; Gellatly and Lyons, 2005; Kaufman et al., 2007) but significantly lower than Cenozoic values (Burdett et al., 1989; Staudt and Schoonen, 1995). The broad consistency of CAS concentrations in Precambrian carbonates, including dolostones and limestones, suggests that large-scale secular trends in CAS concentration and $\delta^{34}S_{CAS}$ are not completely obliterated by dolomitization and confirms the proposition that sulfate concentrations in Proterozoic oceans were generally lower than in Cenozoic oceans (Pavlov et al., 2003).

Although more studies are needed to understand the effect of dolomitization on $\delta^{34}S_{CAS}$, geochemical data from the Zhamoketi cap dolostone seem to suggest that $\delta^{34}S_{CAS}$ values were not strongly altered during dolomitization. The correlations between $\delta^{34}S_{CAS}$ values and Mg/Ca ratios (Fig. 5f) and between $\delta^{34}S_{CAS}$ values and CAS concentrations (Fig. 5b) are both very weak, suggesting no systematic alteration of $\delta^{34}S_{CAS}$ signature during dolomitization or CAS loss.

5.3. Using $\delta^{34}S_{CAS}$ as a proxy for seawater sulfate

CAS is structurally incorporated in the lattice of carbonate minerals, replacing the CO_3^{2-} anions (Pingitore et al., 1995). It has been widely used as a proxy for seawater sulfate $\delta^{34}S$ compositions, especially in Precambrian successions where evaporite rocks are rare (Kampschulte et al., 2001; Hurtgen et al., 2002, 2004, 2006; Kah et al., 2004; Kampschulte and Strauss, 2004; Gellatly and Lyons, 2005; Bottrell and Newton, 2006). Comparisons between sulfur isotope compositions of CAS and co-occurring evaporites reveal only small differences (<5‰) (Burdett et al., 1989; Kah et al., 2004; Kampschulte and Strauss, 2004; Lyons et al., 2004), supporting the use of CAS as a reasonable $\delta^{34}S$ proxy as long as carbonate precipitates are equilibrated with seawater and their diagenetic history is carefully evaluated.

The Zhamoketi cap dolostone was probably deposited below storm wave base. Microsparites and peloids (constituents of macropeloids) in the cap dolostone were likely precipitated in surface water and then settled to the ocean bottom. Diagenetic cements precipitated from pore-water are volumetrically small (<10%; Fig. 3c). Thus, we regard the Zhamoketi $\delta^{34}S_{CAS}$ values as a reasonable proxy for surface seawater $\delta^{34}S$.

5.4. Evaluation of $\delta^{34}S_{py}$ values

The chromium reduction method has been used widely in pyrite extraction (Canfield et al., 1986). The extraction procedure does not introduce any significant isotopic fractionation (Newton et al., 1995). Our experiment with pure pyrite also shows that the procedure

did not introduce significant fractionation ($\delta^{34}S_{Ag2S}$ = +2.6‰ vs. $\delta^{34}S_{py}$ = +1.9‰).

Pyrites exist in the Zhamoketi cap dolostone as disseminated subeuhedral crystals <10 μm in size (Fig. 3e–f). Their distribution is not associated with any microveins or other hydrothermal activities. Certainly, the formation of disseminated pyrites in the Zhamoketi cap dolostone occurred in an anoxic environment where bacterial sulfate reduction took place and reactive iron supply was available. They could have formed during early diagenesis below water-sediment interface or syngenetically in bottom water (e.g., in a sulfate minimum zone). Thus, their $\delta^{34}S_{py}$ values could reflect the isotopic signatures of local environments. Nonetheless, their $\delta^{34}S_{py}$ values are still useful in understanding the sulfur cycle even if they formed in a semi-closed system below the water-sediment interface. In such a system, sulfur isotope fractionation should be limited and $\delta^{34}S_{py}$ values of bulk samples should approach $\delta^{34}S$ of seawater. Many Zhamoketi samples, however, are characterized by $\delta^{34}S_{py}$ values greater than co-occurring $\delta^{34}S_{CAS}$ values (i.e., negative $\Delta\delta^{34}S_{CAS-py}$ values), posing a challenge in their interpretation.

6. Implications for sulfur cycling in the Quruqtagh basin

In our interpretation, we focus on two important features of the $\delta^{34}S$ of the Zhamoketi cap dolostone: the strong stratigraphic variation in $\delta^{34}S$ (in sharp contrast to the stable $\delta^{13}C$ values) and the negative $\Delta\delta^{34}S_{CAS-py}$ values. The rapid stratigraphic variation in $\delta^{34}S_{CAS}$ and $\delta^{34}S_{sulfide}$ of Proterozoic carbonates, along with generally low CAS concentrations, has been interpreted as evidence for a relatively small sulfate reservoir (Pavlov et al., 2003; Kah et al., 2004; Hurtgen et al., 2005; Gellatly and Lyons, 2005; Lyons et al., 2006). This is also a reasonable interpretation for the Zhamoketi cap dolostone. With a generally small sulfate reservoir, the isotopic signature would be more susceptible to local perturbations (e.g., weathering input and upwelling), and there would be frequent development of spatial and depth heterogeneity. All these would contribute to the rapid stratigraphic variation in $\delta^{34}S_{CAS}$ values. The stratigraphic and spatial variations imply that $\delta^{34}S_{CAS}$ and $\delta^{34}S_{py}$ profiles are less useful in chemostratigraphic correlation than $\delta^{13}C$ data.

The negative $\Delta\delta^{34}S_{CAS-py}$ values (Fig. 4f) are puzzling. The formation of sedimentary pyrites is directly related to bacterial sulfate reduction. Experimental data show that the isotopic effect of bacterial sulfate reduction ranges from 2‰ to 42‰ (Detmers et al., 2001). Additional fractionation beyond 42‰ is associated with the disproportionation of intermediate sulfur species (Canfield and Thamdrup, 1994). Thus, sedimentary pyrites are generally expected to be isotopically lighter than contemporaneous seawater sulfate. However, many Mesoproterozoic and Neoproterozoic successions are characterized by highly variable $\delta^{34}S_{py}$ values, some of which exceed the $\delta^{34}S_{CAS}$ values of contemporaneous carbonate (Ross et al., 1995; Canfield, 1998; Gorjan et al., 2000; Hurtgen et al., 2002; Strauss, 2002; Lyons et al., 2006; Liu et al., 2006). $\delta^{34}S_{py}$ values approaching contemporaneous $\delta^{34}S_{CAS}$ values have been interpreted as resulting from bacterial sulfate reduction in sulfate-limited environments (e.g., closed system below water-sediment interface; Strauss, 2002). However, $\delta^{34}S_{py}$ values exceeding contemporaneous $\delta^{34}S_{CAS}$ values were largely ignored by previous authors, because they cannot be easily explained by traditional models where pore-water sulfate for pyrite formation is derived from a homogenous seawater sulfate reservoir. Although the instantaneous sulfide product from bacterial sulfate reduction in a nearly closed system could be isotopically heavier than seawater sulfate, the cumulative sulfide product is not expected to be isotopically heavier than seawater sulfate. The $\delta^{34}S_{py}$ and $\delta^{34}S_{CAS}$ data reported in this paper and from many other Proterozoic successions were from bulk analyses, and the isotopic values are supposed to reflect cumulative rather than instantaneous products. Thus, the negative $\Delta\delta^{34}S_{CAS-py}$ values of the Zhamoketi cap dolostone remain enigmatic.

In order to explain the negative $\Delta\delta^{34}S_{CAS-py}$ values, we hypothesize that Zhamoketi CAS and pyrite were derived from isotopically distinct sulfur reservoirs. In searching for possible processes involved in the sulfur cycling of the post-glacial Quruqtagh basin, we consider the following two models, both of which are related to the generally low sulfate concentrations and isotopic heterogeneity.

6.1. Oceanic stratification model

During the Marinoan glaciation, glaciers existed in tropical oceans (Evans, 2000), and the polar regions were likely completely frozen. As a result, the global ocean conveyor system was probably slowed down, regardless whether the tropical oceans were completely frozen or remained open (Hyde et al., 2000). With reduced polar down-welling, oxygen and sulfate fluxes to the bottom ocean would be reduced. Continuing respiration and bacterial sulfate reduction in the bottom ocean, fueled by a large reservoir of dissolved organic carbon (Rothman et al., 2003) and syn-glacial bioproductivity, would

progressively deplete the oxygen and sulfate levels in the bottom ocean. With sufficient reactive iron input (as indicated by the high Fe concentration in the Zhamoketi cap dolostone), isotopically light H_2S would be removed from the bottom ocean, raising the $\delta^{34}S_{sulfate}$ of residual sulfate reservoir. In the mean time, significant amount of isotopically light DIC (dissolved inorganic carbon) would be produced. Thus, the bottom ocean relic from the Tereeken glaciation would be characterized by anoxia, low sulfate concentration, high $\delta^{34}S_{sulfate}$, and low $\delta^{13}C_{DIC}$ (Fig. 6a).

Upon deglaciation, warm meltwater formed a plume on cold relict bottom water, maintaining physical and chemical stratification for $>10^3$ years (Shields, 2005; Hoffman et al., 2007). The geochemistry of the meltwater plume (or surface water) would be dominated by oxidative weathering of pyrite, evaporite, organic carbon, and silicate minerals. Due to accelerated post-glacial weathering, significant amount of sulfate and DIC would be delivered to oxygenated surface waters, where sulfate reduction is prohibited. Using modern weathering fluxes as a guide ($\delta^{34}S_{weathering}=+6‰$, $\delta^{13}C_{weathering}=-5‰$) (Kump, 1991; Kah et al., 2004), the post-glacial meltwater plume would be generally characterized by moderate sulfate concentration, low $\delta^{34}S_{sulfate}$, and low $\delta^{13}C_{DIC}$ (Fig. 6b).

If the Zhamoketi cap dolostone was deposited below storm wave base, as indicated by the lack of wave affected sedimentary structures, then it was probably deposited below the pycnocline that separates the meltwater plume and bottom water. We hypothesize that, in a stratified basin, the Zhamoketi carbonate and CAS were derived from surface water, recording low $\delta^{34}S_{CAS}$, low $\delta^{13}C_{carb}$, and moderate CAS concentrations. Petrographic observations are consistent with this hypothesis. Zhamoketi microsparites and peloids likely formed in the surface water probably as pelagic carbonate; benthic carbonate such as cements is volumetrically insignificant (Fig. 3c).

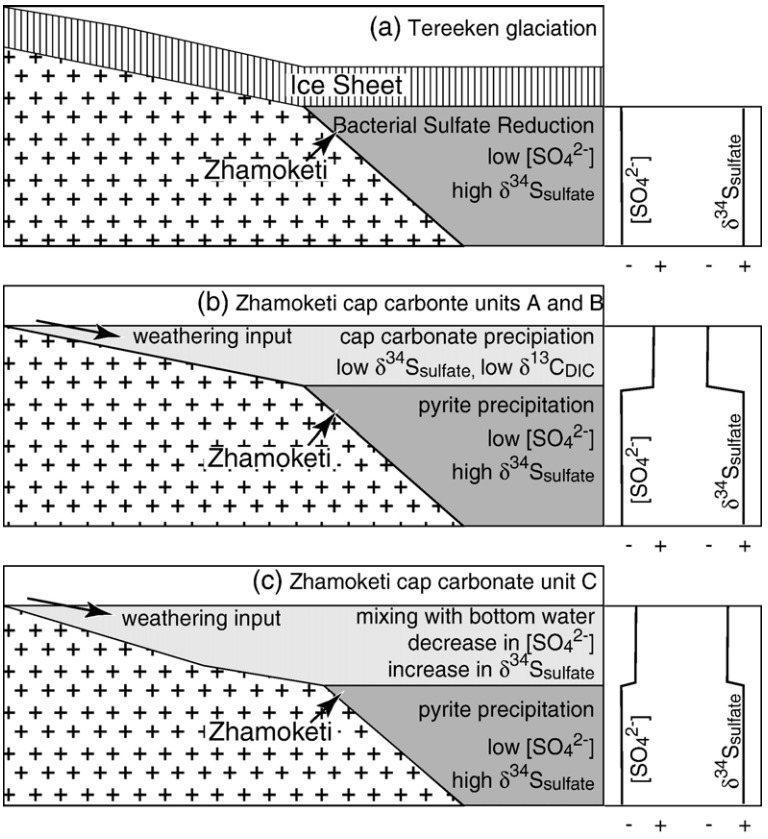

Fig. 6. Basin stratification model. (a) During the Tereeken glaciation, basin was covered by ice sheet and bacterial sulfate reduction was active in bottom water, leading to lower SO_4^{2-} concentrations and higher $\delta^{34}S_{sulfate}$ values. (b) During early deglaciation (Zhamoketi cap carbonate unit A and B), meltwater plume maintained basin stratification. Weathering input led to moderate SO_4^{2-} concentrations and low $\delta^{34}S_{sulfate}$ values in surface water. It is hypothesized that cap carbonate and CAS were derived from surface water, whereas sulfur source for pyrite formation came from bottom water. (c) During late deglaciation (Zhamoketi cap carbonate unit C), partial mixing led to higher $\delta^{34}S_{sulfate}$ and lower sulfate concentration in surface water.

As the $\delta^{34}S_{CAS}$ values have not been strongly altered by diagenesis (see above discussion), we infer that either the Zhamoketi cap carbonate was precipitated as primary dolomite or its $\delta^{34}S_{CAS}$ values were buffered against secondary dolomitization.

In contrast, sulfur available for pyrite formation was derived from anoxic bottom water characterized by high $\delta^{34}S$ values due to long-term syn-glacial sulfate reduction. $\delta^{34}S_{py}$ can thus approach and exceed $\delta^{34}S_{CAS}$ derived from surface water, particularly if pyrite formation occurred in a semi-closed system below the water-sediment interface.

Calculation based on a Rayleigh distillation model shows that about 30–85% depletion of the bottom water sulfate reservoir by sulfate reduction is required to produce the observed sulfur isotope signature of the Zhamoketi cap dolostone (Fig. 7). This is calculated as follows. If bottom water sulfate was the ultimate sulfur source of Zhamoketi pyrite, the observed average $\delta^{34}S_{py}$ value of 15.8‰ requires a bottom water $\delta^{34}S_{sulfate}$ value of 50.8‰ assuming a cumulative isotopic fractionation of 35‰ by sulfate reduction bacteria (SRB)—a conservative assumption because the cumulative fractionation was likely much less than 35‰ due to sulfate limitation. This indicates 30–85% syn-glacial depletion of bottom water sulfate by SRB, depending on pre-glacial $\delta^{34}S_{sulfate}$ value (e.g. +30‰; Shields et al., 2007) and the instantaneous isotopic fractionation factor by SRB. In comparison, the observed average $\delta^{34}S_{CAS}$ value is +13.4‰, requiring that weathering influx ($\delta^{34}S_{weathering}$=+6‰) contributed roughly 50–70% of surface water sulfate reservoir depending on pre-glacial $\delta^{34}S_{sulfate}$ value (Fig. 7).

The stratification model brings up two questions. First, what drove the sulfur isotope distillation of the bottom ocean? Presumably, organic carbon for bacterial sulfate reduction was supplied by a large DOC reservoir (Rothman et al., 2003) and possible syn-glacial bioproduction (Corsetti et al., 2003). Syn-glacial bioproduction may have occurred in potentially open tropic oceans (Hyde et al., 2000) or during intermittently thawing periods (as suggested by the siltstones interbedded with diamictites of the Zhamoketi Formation). However, syn-glacial sulfate replenishment to the deep ocean was minimal because of reduced polar downwelling. These factors, together with the low sulfate concentrations in Proterozoic oceans to begin with, make it theoretically possible to deplete deep-water sulfate by 30–85% if the basin was stratified. Another question relates to the low pyrite concentrations in the Zhamoketi cap dolostone. Why pyrite concentrations are low if 30–85% deep-water sulfate was consumed by sulfate reduction bacteria? Reactive iron does not appear to have imposed a limitation on pyrite formation,

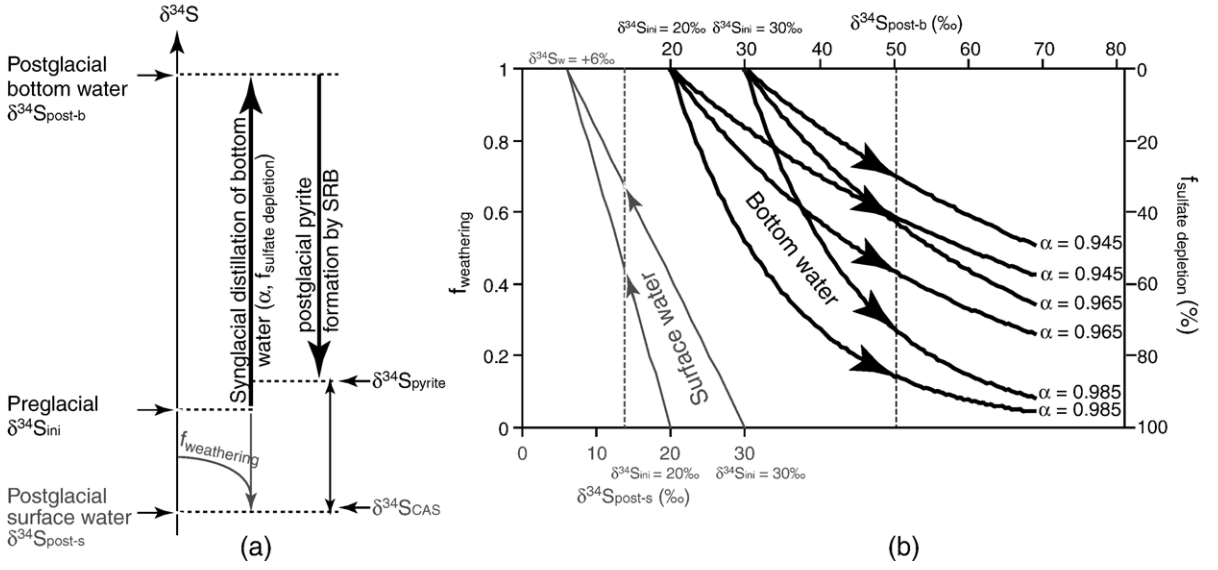

Fig. 7. (a) Schematic diagram showing $\delta^{34}S_{sulfate}$ evolution in the surface water (thin grey lines) and bottom water (thick solid lines) during and after the Tereeken glaciation. (b) Post-glacial weathering flux to surface water (thin grey lines) and syn-glacial distillation of bottom water by sulfate reduction (thick solid lines) necessary to explain observed sulfur isotopes (average $\delta^{34}S_{CAS}$=+13.4‰; average $\delta^{34}S_{py}$=+15.8‰; dotted lines) of the Zhamoketi cap dolostone based on the basin stratification model. As a sensitivity test, calculation was made assuming an initial pre-glacial $\delta^{34}S_{sulfate}$ value of +20‰ and +30‰, and a fractionation factor (α) of 0.945, 0.965, and 0.985.

because iron concentrations are generally high. We argue that low pyrite concentrations are related to the generally low sulfate availability in Proterozoic oceans. In addition, the rapid sedimentation rate of the cap carbonate (Hoffman et al., 1998) may have also played a role in diluting pyrite concentrations.

It is uncertain how long the basin stratification lasted. However, there is evidence for some degree of mixing at about 2.5 m. Below 2.5 m, $\delta^{34}S_{CAS}$ values are consistently lower than $\delta^{34}S_{py}$ values, a pattern that could be explained by the stratification model described above. Above 2.5 m, however, the overall range of $\delta^{34}S_{CAS}$ values encompass the $\delta^{34}S_{py}$ range although individual samples have $\delta^{34}S_{CAS} < \delta^{34}S_{py}$. We interpret the overlapping $\delta^{34}S_{CAS}$ and $\delta^{34}S_{py}$ ranges as evidence for partial mixing of surface and bottom waters (Fig. 6c). After mixing, sulfate concentration would decrease while $\delta^{34}S$ increases in surface water. This is consistent with the stratigraphic increase in average $\delta^{34}S_{CAS}$ at about 2.5 m. The decrease in CAS, however, occurs lower in stratigraphy (~1 m), and it is uncertain whether the stratigraphic offset is geochronologically significant because of the uncertainty in sedimentation rate. $\delta^{34}S_{py}$ values, on the other hand, would not be affected as much as $\delta^{34}S_{CAS}$ by the mixing if sulfur source for pyrite formation was consistently derived from anoxic deep waters.

If partial mixing occurred around 2.5 m, why wasn't the $\delta^{13}C_{carb}$ signature disturbed at the same level? Negative $\delta^{13}C_{carb}$ values of cap dolostones atop Marinoan glacial deposits have been interpreted in terms of post-glacial overturn of a ^{12}C-enriched deep ocean (Knoll et al., 1986, 1996; Kaufman et al., 1991; Grotzinger and Knoll, 1995), Rayleigh distillation of a large atmospheric CO_2 reservoir (Hoffman et al., 1998), release of isotopically light gas hydrates (Kennedy et al., 2001; Jiang et al., 2003), catastrophic temperature rise and kinetic isotopic effect associated with rapid carbonate sedimentation (Higgins and Schrag, 2003). Perhaps all of these processes may have contributed to the $\delta^{13}C_{carb}$ pattern. But if both the meltwater plume and bottom water are characterized by similarly negative $\delta^{13}C_{carb}$ values, the partial mixing at 2.5 m would not have significant impact on the $\delta^{13}C_{carb}$ values of the cap dolostone. This is particularly true if the surface ocean represented a high alkalinity source and had a stronger buffer against disturbance than the sulfur system. Even so, the negative stratigraphic trend of $\delta^{13}C_{carb}$ in many Marinoan cap dolostones (Kennedy et al., 1998; Zhou and Xiao, 2007) may record an oceanic mixing between surface and bottom waters (Kaufman et al., 1991; Grotzinger and Knoll, 1995; Knoll et al., 1996).

Because of the uniqueness of Neoproterozoic global glaciations, a modern analog to the stratification model would not be expected. Nonetheless, the euxinic fjord at Framvaren of southern Norway may shed some light on the stratification model. Pyrite in the bottom sediments of the Framvaren fjord is enriched in ^{34}S, reaching $\delta^{34}S_{py}$ values around −12‰, compared with values around −35‰ near and above the chemocline (Sælen et al., 1993). This enrichment was interpreted as a result of intense bacterial reduction in the bottom water whose exchange with the open ocean is limited by shallow sills and a surface lid of low-salinity meltwater. Of course, despite their negative $\Delta\delta^{34}S_{sulfate-py}$ values, Framvaren pyrites are not as ^{34}S-enriched as Zhamoketi pyrites. However, with (1) a smaller sulfate reservoir in the Neoproterozoic ocean, (2) prolonged syn-glacial bacterial sulfate reduction, (3) sufficient reactive iron to titrate sulfide from the bottom water, and (4) continuing post-glacial stratification, the residual sulfate and hence pyrite derived from in the Zhamoketi bottom water would be much more ^{34}S-enriched than the Framvaren fjord.

A similar stratification model has been proposed by Holser (1977) to explain superheavy $\delta^{34}S_{py}$ values at the Neoproterozoic–Cambrian, middle–late Devonian, and early–middle Triassic transitions. In Holser's model, oceanic stratification in more or less restricted basins is induced by brine formation in evaporitic environments. Evaporitic brines stored in deep basins are subjected to isotopic distillation by sulfate reduction bacteria, driving the sulfur isotope of residual sulfate to greater values. Catastrophic overturn of deep-water brines would introduce ^{34}S-enriched sulfate into the surface water, leading to the precipitation of ^{34}S-enriched pyrites. A general theme of these models is chemical stratification, the isolation of a ^{34}S-enriched sulfate pool in the bottom water, and subsequent oceanic overturn resulting in the observed sulfur isotopic patterns.

6.2. Sulfate minimum zone model

Inspired by Logan et al. (1995), we also consider an alternative model in which the ^{34}S-enriched sulfate pool is not isolated in the bottom water, but in a sulfate minimum zone (SMZ). Indeed, the SMZ model has been used to explain the generally heavy $\delta^{34}S_{sulfide}$ values that exceed corresponding $\delta^{34}S_{sulfate}$ values in Neoproterozoic rocks (Logan et al., 1995; Li et al., 1999). In this model, no oceanic stagnation is required. The oceanic conveyor system would operate as in modern oceans, delivering oxygen and sulfate to the deep ocean. However, because of the generally low sulfate concentration

in Neoproterozoic oceans, sulfate could be overwhelmed by settling organic carbon, creating a SMZ analogous to the oxygen minimum zone in the modern ocean (Logan et al., 1995). In this SMZ, intense bacterial sulfate reduction would deplete sulfate and drive $\delta^{34}S_{sulfate}$ to greater values (Fig. 8a). The SMZ would be likely below the storm wave base. Where the SMZ encroached the continental shelf or slope, its ^{34}S-enriched sulfate pool would become the source of pore water sulfate reduction, leading to the formation of ^{34}S-enriched pyrite. Alternatively, pyrite formation could also occur syngenetically in the anoxic SMZ. Thus, at least the lowermost 2.5 m of the Zhamoketi cap dolostone represent deposition at or beneath the SMZ, with carbonate and CAS derived from surface water, and sulfur for pyrite formation from the SMZ. Above 2.5 m, partial decay of the SMZ may be responsible for the slight change in $\Delta\delta^{34}S_{CAS-py}$ values (Fig. 8b).

These models should be tested with more geochemical data from other cap dolostones. Unfortunately, high-resolution paired $\delta^{34}S_{CAS}$ and $\delta^{34}S_{py}$ analyses of carbonates equivalent to the Zhamoketi cap dolostone are still sporadic and systematic $\delta^{34}S_{CAS}$ data are only available for the Maieberg Formation in Namibia (Hurtgen et al., 2002, 2006), Noonday Dolomite in Death Valley (Hurtgen et al., 2004), Jbeliat cap carbonate in the Taoudéni Basin (Shields et al., 2007), and the Doushantuo cap dolostone in South China (Zhang et al., 2003; Goldberg et al., 2005). Although their thickness varies significantly (Hoffman et al., 2007), several Marinoan cap dolostones are characterized by a 3–15‰ positive $\delta^{34}S_{CAS}$ shift in the lowermost part (arrows in Fig. 9), similar to the positive shift (~5‰) in the basal Zhamoketi cap dolostone. However, systematic and concurrent $\delta^{34}S_{py}$ analyses have not been carried out for these successions and a comparative study between the Zhamoketi and other Ediacaran cap dolostones is premature.

Nonetheless, available $\delta^{34}S_{CAS}$ data from basal Ediacaran cap carbonates show strong spatial and stratigraphic variations (Fig. 9), in sharp contrast to the consistently negative $\delta^{13}C_{carb}$ values (Kennedy et al., 1998; Zhou and Xiao, 2007). The variations speak to the generally small sulfate reservoir in post-glacial oceans and the volatility of the $\delta^{34}S_{sulfate}$ signatures that were subject to local disturbance including riverine and upwelling input. In light of this, it is not surprising that there may have been a significant onshore-offshore $\delta^{34}S_{sulfate}$ gradient (Hurtgen et al., 2006). As would be expected, $\delta^{34}S_{CAS}$ values of the Zhamoketi cap dolostone (+9.1‰ to +20.6‰), which was deposited in relatively deep-water environment below storm wave base, would be more akin to those of open shelf sections (section MS-3: +15.2‰ to +24.1‰; section MS-8:

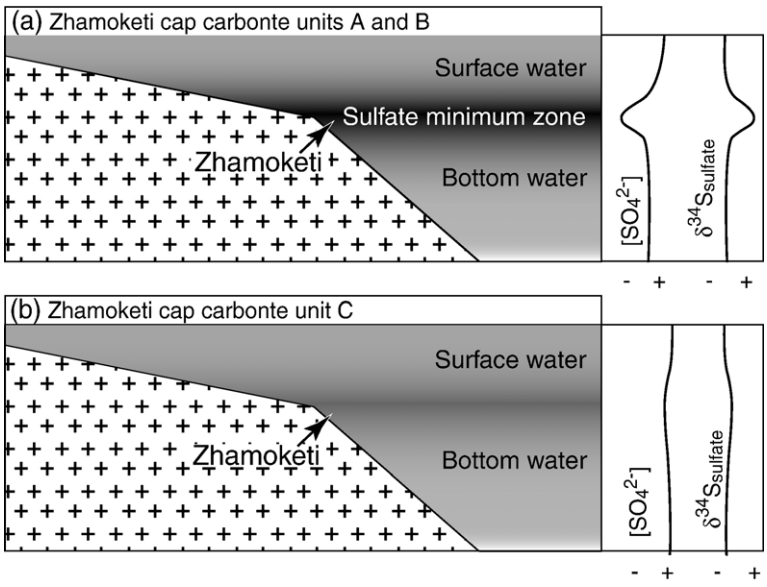

Fig. 8. Sulfate minimum zone model. (a) A sulfate minimum zone was formed due to slow sinking rate of organic carbon (Logan et al., 1995). Isotopic distillation in the sulfate minimum zone led to low SO_4^{2-} concentrations and elevated $\delta^{34}S_{sulfate}$ values. It is hypothesized that carbonate and CAS in Zhamoketi cap dolostone units A–B were derived from surface water, whereas sulfur for pyrite formation came from the sulfate minimum zone. (b) Attenuation of the sulfate minimum zone led to partial mixing and increased $\delta^{34}S_{sulfate}$ values in surface water during the precipitation of Zhamoketi cap carbonate unit C.

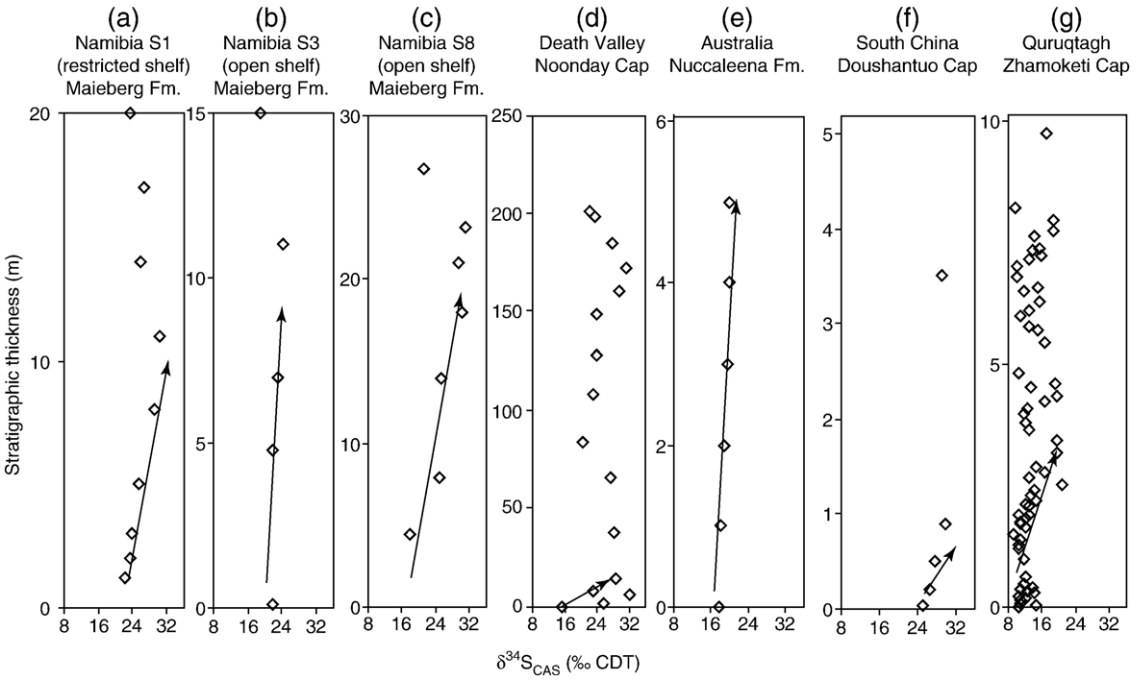

Fig. 9. Comparison of $\delta^{34}S_{CAS}$ profiles of supposedly equivalent cap carbonate following the Marinoan glaciation. (a–c) Keiberg cap dolostone, Namibia (Hurtgen et al., 2006). Section S1, restricted shelf. Sections S3 and S8, open shelf. (d) Noonday cap carbonate, Death Valley (Hurtgen et al., 2004). (e) Nuccaleena cap dolostone, South Australia (Hurtgen et al., 2005). (f) Doushantuo cap dolostone, South China (Zhang et al., 2003). (g) Zhamoketi cap dolostone, Quruqtagh (this paper). Arrows indicates positive $\delta^{34}S_{CAS}$ shift in basal cap carbonates.

+15.5‰ to +44.8‰) than restricted shelf sections (MS-1: +19.3‰ to +47.0‰) of the Maieberg Formation in Namibia (Hurtgen et al., 2006).

7. Conclusions

Systematic sulfur isotope analysis of the basal Ediacaran Zhamoketi cap dolostone shows that $\delta^{34}S_{py}$ values are within ±10‰ of corresponding $\delta^{34}S_{CAS}$ values, and in most samples $\delta^{34}S_{py}$ is greater than corresponding $\delta^{34}S_{CAS}$. The negative $\Delta\delta^{34}S_{CAS-py}$ values, calculated from $\delta^{34}S_{CAS}$ and $\delta^{34}S_{py}$ analyses of bulk samples, are inconsistent with derivation of sulfate and sulfide from the same sulfur reservoir. Instead, CAS and pyrite were likely derived from two isotopically distinct reservoirs in a chemically stratified basin. In this model, CAS is hypothesized to have been derived from oxic surface water with moderate sulfate concentration, lower $\delta^{34}S_{sulfate}$ (due to post-glacial, oxidative weathering of pyrite), and lower $\delta^{13}C_{DIC}$. In contrast, sulfur for pyrite formation may have come from anoxic bottom water that was relict from the Marinoan glaciation and was characterized by lower sulfate concentration, higher $\delta^{34}S_{sulfate}$ (due to limited sulfate supply, continuing sulfate reduction, and pyrite precipitation during the Marinoan glaciation), and lower $\delta^{13}C_{DIC}$ (due to production of alkalinity associated with sulfate reduction). Alternatively, the Quruqtagh basin was not chemically stratified, but pyrites were formed in a sulfate minimum zone. In either case, it appears that oceanic mixing occurred about 2.5 m, where $\delta^{34}S_{CAS}$ and $\delta^{34}S_{py}$ values begin to converge.

The spatial heterogeneity and temporal variations in $\delta^{34}S_{CAS}$ and $\delta^{34}S_{py}$, as well as the possibility for the bottom water sulfate reservoir to be isotopically distilled during stratification, indicate relatively low sulfate concentration in post-glacial oceans. Because of the heterogeneity, care must be taken when applying $\delta^{34}S$ data in chemostratigraphic correlation of Proterozoic successions.

Acknowledgments

This work was supported by grants from National Science Foundation (EAR-0545135 and EAR 0418005), NASA Exobiology Program (NNG05GP21G and NNG05GP36G), Petroleum Research Foundation (42231-AC8), National Natural Science Foundation of China (40628002), Chinese Academy of Sciences (KZCX-SW-141), and Chinese Ministry of Science and Technology (2006CB806400). We thank Y. Qian, J. Wang, and L.

Zhang for field assistance; N. Han, A. M. Tilley, and J. Liu for laboratory assistance; X. Yuan, G. Jiang, T. W. Lyons, X. Chu, and an anonymous reviewer for constructive comments.

References

Allen, P.A., Hoffman, P.F., 2005. Extreme winds and waves in the aftermath of a Neoproterozoic glaciation. Nature 433, 123–127.

Bottrell, S.H., Newton, R.J., 2006. Reconstruction of changes in global sulfur cycling from marine sulfate isotopes. Earth Sci. Rev. 75, 59–83.

Burdett, J., Authur, M., Richardson, M., 1989. A Neogene seawater sulfur isotope age curve from calcareous pelagic microfossils. Earth Planet. Sci. Lett. 94, 189–198.

Canfield, D.E., 1998. A new model for Proterozoic ocean chemistry. Nature 396, 450–453.

Canfield, D.E., Thamdrup, B., 1994. The production of ^{34}S-depleted sulfide during bacterial disproportionation of elemental sulfur. Science 266, 1973–1975.

Canfield, D.E., Raiswell, R., Westrich, J.T., Reaves, C.M., Berner, R.A., 1986. The use of chromium reduction in the analysis of reduced inorganic sulfur in sediments and shales. Chem. Geol. 54, 149–155.

Condon, D., Zhu, M., Bowring, S., Wang, W., Yang, A., Jin, Y., 2005. U–Pb Ages from the Neoproterozoic Doushantuo Formation, China. Science 308, 95–98.

Corsetti, F.A., Grotzinger, J.P., 2005. Origin and significance of tube structures in Neoproterozoic post-glacial cap carbonates: example from Noonday Dolomite, Death Valley, United States. Palaios 20, 348–362.

Corsetti, F.A., Lorentz, N.J., 2006. On Neoproterozoic cap carbonate as chronostratigraphic markers. In: Xiao, S., Kaufman, A.J. (Eds.), Neoproterozoic Geobiology and Paleobiology. Springer, Dordrecht, pp. 273–294.

Corsetti, F.A., Awramik, S.M., Pierce, D., 2003. A complex microbiota from snowball Earth times: microfossils from the Neoproterozoic Kingston Peak Formation, Death Valley, USA. Proc. Nat. Acad. Sci. U. S. A. 100, 4399–4404.

Detmers, J., Brüchert, V., Habicht, K.S., Kuever, J., 2001. Diversity of sulfur isotope fractionations by sulfate-reducing prokaryotes. Appl. Environ. Microbiol. 67, 888–894.

Evans, D.A.D., 2000. Stratigraphic, geochronological, and paleomagnetic constraints upon the Neoproterozoic climatic paradox. Am. J. Sci. 300, 347–433.

Fike, D.A., Grotzinger, J.P., Pratt, L.M., Summons, R.E., 2006. Oxidation of the Ediacaran ocean. Nature 444, 744–747.

Gao, Z., Zhu, S., 1984. Precambrian Geology in Xinjiang, China. Xinjiang People's Publishing House, Urumuqi, China.

Gao, Z., Peng, C., Li, Y., Qian, J., Zhu, S., 1980. The Sinian System and its glacial deposits in Quruqtagh, Xinjiang, in: Tianjin Institute of Geology and Mineral Resources (Ed.), Research in Precambrian Geology, Sinian Suberathem in China. Tianjin Science and Technology Press, Tianjin, pp. 186–213.

Gao, Z., Chen, J., Lu, S., Peng, C., Qin, Z., 1993. The Precambrian Geology in Northern Xinjiang (Precambrian Geology No. 6). Geological Publishing House, Beijing.

Gellatly, A.M., Lyons, T.W., 2005. Trace sulfate in mid-Proterozoic carbonates and the sulfur isotope record of biospheric evolution. Geochim. Cosmochim. Acta 69, 3813–3829.

Goldberg, T., Poulton, S.W., Strauss, H., 2005. Sulphur and oxygen isotope signatures of late Neoproterozoic to early Cambrian sulphate, Yangtze Platform, China: diagenetic constraints and seawater evolution. Precambrian Res. 137, 223–241.

Gorjan, P., Veevers, J.J., Walter, M.R., 2000. Neoproterozoic sulfur-isotope variation in Australia and global implications. Precambrian Res. 100, 151–179.

Grassineau, N.V., Mattey, D.P., Lowry, D., 2001. Sulfur isotope analysis of sulfide and sulfate minerals by continuous flow-isotope ratio mass spectrometry. Anal. Chem. 73, 220–225.

Grotzinger, J.P., Knoll, A.H., 1995. Anomalous carbonate precipitates: is the Precambrian the key to the Permian? Palaios 10, 578–596.

Halverson, G.P., 2006. A Neoproterozoic chronology. In: Xiao, S., Kaufman, A.J. (Eds.), Neoproterozoic Geobiology and Paleobiology. Springer, Dordrecht, pp. 232–271.

Halverson, G.P., Hoffman, P.F., Schrag, D.P., Maloof, A.C., Rice, A.H.N., 2005. Toward a Neoproterozoic composite carbon-isotope record. Geol. Soc. Am. Bull. 117, 1181–1207.

Higgins, J.A., Schrag, D.P., 2003. Aftermath of a snowball Earth. Geochem. Geophys. Geosys. 4 (G3). doi:10.1029/2002GC000403 (Article Number 1028).

Hoffman, P.F., Schrag, D.P., 2002. The snowball Earth hypothesis: testing the limits of global change. Terra Nova 14, 129–155.

Hoffman, P.F., Kaufman, A.J., Halverson, G.P., Schrag, D.P., 1998. A Neoproterozoic snowball Earth. Science 281, 1342–1346.

Hoffmann, K.-H., Condon, D.J., Bowring, S.A., Crowley, J.L., 2004. U–Pb zircon date from the Neoproterozoic Ghaub Formation, Namibia: constraints on Marinoan glaciation. Geology 32, 817–820.

Hoffman, P.F., Halverson, G.P., Domack, E.W., Husson, J.M., Higgins, J.A., Schrag, D.P., 2007. Are basal Ediacaran (635 Ma) post-glacial "cap dolostones" diachronous? Earth Planet. Sci. Lett. 258, 114–131.

Holser, W.T., 1977. Catastrophic chemical events in the history of the ocean. Nature 267, 403–408.

Hurtgen, M.T., Arthur, M.A., Suits, N.S., Kaufman, A.J., 2002. The sulfur isotopic composition of Neoproterozoic seawater sulfate: implications for a snowball Earth? Earth Planet. Sci. Lett. 203, 413–429.

Hurtgen, M.T., Arthur, M.A., Prave, A.R., 2004. The sulfur isotope composition of carbonate-associated sulfate in Mesoproterozoic to Neoproterozoic carbonates from Death Valley, California. In: Amend, J.P., Edwards, K.J., Lyons, T.W. (Eds.), Sulfur Biogeochemistry—Past and Present. Geological Society of America Special Paper, vol. 379, pp. 177–194.

Hurtgen, M.T., Arthur, M.A., Halverson, G.P., 2005. Neoproterozoic sulfur isotopes, the evolution of microbial sulfur species, and the burial efficiency of sulfide as sedimentary pyrite. Geology 33, 41–44.

Hurtgen, M.T., Halverson, G.P., Arthur, M.A., Hoffman, P.F., 2006. Sulfur cycling in the aftermath of a 635-Ma snowball glaciation: evidence for a syn-glacial sulfidic deep ocean. Earth Planet. Sci. Lett. 245, 551–570.

Hyde, W.T., Crowley, T.J., Baum, S.K., Peltier, W.R., 2000. Neoproterozoic "snowball Earth" simulations with a coupled climate/ice-sheet model. Nature 405, 425–429.

James, N.P., Narbonne, G.M., Kyser, T.K., 2001. Late Neoproterozoic cap carbonates: Mackenzie Mountains, Northwestern Canada: precipitation and global glaciation meltdown. Can. J. Earth Sci. 38, 1229–1262.

Jiang, G., Kennedy, M.J., Christie-Blick, N., 2003. Stable isotopic evidence for methane seeps in Neoproterozoic postglacial cap carbonates. Nature 426, 822–826.

Jiang, G., Kennedy, M.J., Christie-Blick, N., Wu, H., Zhang, S., 2006. Stratigraphy, sedimentary structures, and textures of the Late Neoproterozoic Doushantuo cap carbonate in South China. J. Sediment. Res. 76, 978–995.

Kah, L.C., Lyons, T.W., Frank, T.D., 2004. Low marine sulphate and protracted oxygenation of the Proterozoic biosphere. Nature 431, 834–838.

Kampschulte, A., Strauss, H., 2004. The sulfur isotopic evolution of Phanerozoic seawater based on the analysis of structurally substituted sulfate in carbonates. Chem. Geol. 204, 255–286.

Kampschulte, A., Bruckschen, P., Strauss, H., 2001. The sulphur isotopic composition of trace sulphates in Carboniferous brachiopods: implications for coeval seawater, correlation with other geochemical cycles and isotope stratigraphy. Chem. Geol. 205, 149–173.

Kaufman, A.J., Hayes, J.M., Knoll, A.H., Germs, G.J.B., 1991. Isotopic compositions of carbonates and organic carbon from upper Proterozoic successions in Namibia: stratigraphic variation and the effects of diagenesis and metamorphism. Precambrian Res. 49, 301–327.

Kaufman, A.J., Corsetti, F.A., Varni, M.A., 2007. The effect of rising atmospheric oxygen on carbon and sulfur isotope anomalies in the Neoproterozoic Johnnie Formation, Death Valley, USA. Chem. Geol. 237, 47–63.

Kennedy, M.J., Runnegar, B., Prave, A.R., Hoffmann, K.H., Arthur, M.A., 1998. Two or four Neoproterozoic glaciations? Geology 26 (12), 1059–1063.

Kennedy, M.J., Christie-Blick, N., Sohl, L.E., 2001. Are Proterozoic cap carbonates and isotopic excursions a record of gas hydrate destabilization following Earth's coldest intervals? Geology 29, 443–446.

Knoll, A.H., Hayes, J.M., Kaufman, A.J., Swett, K., Lambert, I.B., 1986. Secular variation in carbon isotope ratios from Upper Proterozoic successions of Svalbard and East Greenland. Nature 321, 832–838.

Knoll, A.H., Bambach, R.K., Canfield, D.E., Grotzinger, J.P., 1996. Comparative earth history and Late Permian mass extinction. Science 273, 452–457.

Kump, L.R., 1991. Interpreting carbon-isotope excursions: strangelove oceans. Geology 19, 299–302.

Leather, J., Allen, P.A., Brasier, M.D., Cozzi, A., 2002. Neoproterozoic snowball Earth under scrutiny: evidence from the Fiq glaciation of Oman. Geology 30, 891–894.

Li, R., Chen, J., Zhang, S., Lei, J., Shen, Y., Chen, X., 1999. Spatial and temporal variations in carbon and sulfur isotopic compositions of Sinian sedimentary rocks in the Yangtze platform, South China. Precambrian Res. 97, 59–75.

Liu, T.-B., Maynard, J.B., Alten, J., 2006. Superheavy S isotopes from glacier-associated sediments of the Neoproterozoic of south China: oceanic anoxia or sulfate limitation? In: Kesler, S.E., Ohmoto, H. (Eds.), Evolution of Early Earth's Atmosphere, Hydrosphere, and Biosphere—Constraints from Ore Deposits: Geological Society of America Memoir 198. Geological Society of America, Boulder, Colorado, pp. 205–222.

Logan, G.A., Hayes, J.M., Hieshima, G.B., Summons, R.E., 1995. Terminal Proterozoic reorganization of biogeochemical cycles. Nature 376, 53–57.

Lyons, T.W., Walter, L.M., Gellatly, A.M., Martini, A.M., Blake, R.E., 2004. Sites of anomalous organic remineralization in the carbonate sediment of South Florida, USA: the sulfur cycle and carbonate-associated sulfate. In: Amend, J.P., Edwards, K.J., Lyons, T.W. (Eds.), Sulfur Biogeochemistry: Past and Present. GSA Special Paper, vol. 379. Geological Society of America, Boulder, Colorado, pp. 161–176.

Lyons, T.W., Hurtgen, M.T., Gill, B.C., 2005. New insight into the utility of carbonate-associated sulfate. Geochim. Cosmochim. Acta 69, A128.

Newton, R.J., Bottrell, S.H., Dean, S.P., Hatfield, D., Raiswell, R., 1995. An evaluation of the use of the chromous chloride reduction method for isotopic analyses of pyrite in rocks and sediment. Chem. Geol. 125, 317–320.

Nédélec, A., Affaton, P., France-Lanord, C., Charrière, A., Alvaro, J., 2007. Sedimentology and chemostratigraphy of the Bwipe Neoproterozoic cap dolostones (Ghana, Volta Basin): a record of microbial activity in a peritidal environment. Comptes Rendus Geosci. 339, 223–239.

Norin, E., 1937. Reports from the Scientific Expedition to the Northwestern Provinces of China under the Leadership of Dr. Sven Hedin, III. Geology of Western Quruqtagh, Eastern Tien-Shan. Bokförlags Aktiebolaget Thule, Stockholm. Geology, vol. 1.

Pavlov, A.A., Hurtgen, M.T., Kasting, J.F., Arthur, M.A., 2003. Methane-rich Proterozoic atmosphere? Geology 31, 87–90.

Pingitore Jr., N.E., Meitzner, G., Love, K.M., 1995. Identification of sulfate in natural carbonates by X-ray absorption spectroscopy. Geochim. Cosmochim. Acta 59, 2477–2483.

Ross, G.M., Bloch, J.D., Krouse, H.R., 1995. Neoproterozoic strata of the southern Canadian Cordillera and the isotopic evolution of seawater sulfate. Precambrian Res. 73, 71–99.

Rothman, D.H., Hayes, J.M., Summons, R.E., 2003. Dynamics of the Neoproterozoic carbon cycle. Proc. Nat. Acad. Sci. U. S. A. 100, 8124–8129.

Sælen, G., Raiswell, R., Talbot, M.R., Skei, J.M., Bottrell, S.H., 1993. Heavy sedimentary sulfur isotopes as indicators of super-anoxic bottom-water conditions. Geology 21, 1091–1094.

Shields, G.A., 2005. Neoproterozoic cap carbonates: a critical appraisal of existing models and the plumeworld hypothesis. Terra Nova 17, 299–310.

Shields, G.A., Deynoux, M., Strauss, H., Paquet, H., Nahon, D., 2007. Barite-bearing cap dolostones of the Taoudéni Basin, northwest Africa: sedimentary and isotopic evidence for methane seepage after a Neoproterozoic glaciation. Precambrian Res. 153, 209–235.

Staudt, W.J., Schoonen, M.A.A., 1995. Sulfate incorporation into sedimentary carbonates. In: Vairavamurthy, M.A., Schoonen, M.A.A. (Eds.), Geochemical Transformations of Sedimentary Sulfur American Chemical Society, pp. 332–345.

Strauss, H., 2002. The isotopic composition of Precambrian sulphides: seawater chemistry and biological evolution. In: Altermann, W., Corcoran, P.L. (Eds.), Precambrian Sedimentary Environments: A Modern Approach to Ancient Depositional Systems (Special Publication Number 33 of the International Association of Sedimentologists). Blackwell Science, Oxford, pp. 67–105.

Xiao, S., Bao, H., Wang, H., Kaufman, A.J., Zhou, C., Li, G., Yuan, X., Ling, H., 2004. The Neoproterozoic Quruqtagh Group in eastern Chinese Tianshan: evidence for a post-Marinoan glaciation. Precambrian Res. 130, 1–26.

Xu, B., Jian, P., Zheng, H., Zou, H., Zhang, L., Liu, D., 2005. U–Pb zircon geochronology and geochemistry of Neoproterozoic volcanic rocks in the Tarim Block of northwest China: implications for the breakup of Rodinia supercontinent and Neoproterozoic glaciations. Precambrian Res. 136 (2), 107–123.

Yao, J., Xiao, S., Yin, L., Li, G., Yuan, X., 2005. Basal Cambrian microfossils from the Yurtus and Xishanblaq formations (Tarim,

north-west China): systematic revision and biostratigraphic correlation of *Micrhystridium*-like acritarchs from China. Palaeontology 48, 687–708.

Zhang, T., Chu, X., Zhang, Q., Feng, L., Huo, W., 2003. Variations of sulfur and carbon isotopes in seawater during the Doushantuo stage in late Neoproterozoic. Chin. Sci. Bull. 48, 1375–1380.

Zhang, C.-L., Li, X.-H., Li, Z.-X., Lu, S.-N., Ye, H.-M., Li, H.-M., 2007. Neoproterozoic ultramafic-mafic-carbonatite complex and granitoids in Quruqtagh of northeastern Tarim Block, western China: geochronology, geochemistry and tectonic implications. Precambrian Res. 152, 149–169.

Zhao, X., Zhang, L., Zou, X., Wang, S., Hu, Y., 1980. Sinian tillites in Northwest China and their stratigraphic significance, in: Tianjin Institute of Geology and Mineral Resources (Ed.), Research on Precambrian Geology Sinian Suberathem in China. Tianjin Science and Technology Press, Tianjin, pp. 164–185.

Zhou, C., Xiao, S., 2007. Ediacaran $\delta^{13}C$ chemostratigraphy of South China. Chem. Geol. 237, 89–108.